# Experimental and Numerical Study of Hydrodynamic Responses of a Combined Wind and Wave Energy Converter Concept in Survival Modes

**Ling Wan[1,2 *], Zhen Gao[1,2,3], Torgeir Moan[1,2,3]**
1. Centre for Ship and Ocean Structures (CeSOS)
2. Norwegian University of Science and Technology (NTNU) Trondheim, Norway
3. Centre for Autonomous Marine Operations and Systems (AMOS)

## 1 Abstract

The Spar Torus Combination (STC) concept combines a spar floating wind turbine and a torus-shaped heaving-body wave energy converter (WEC). Numerical simulations have shown a positive synergy between the WEC and the spar floating wind turbine under operational conditions. However, it is challenging to maintain structural integrity under extreme wind and wave conditions, especially for the WEC. To ensure the survivability of the STC under extreme conditions, three survival modes have been proposed. To investigate the performance of the STC under extreme conditions, model tests with a scaling factor of 1:50 were carried out in the towing tank of MARINTEK, Norway. Two survival modes were tested. In both modes, the torus WEC was fixed to the spar. In the first mode, the torus WEC is at the mean water surface, while in the second mode, it is fully submerged to a specified position. The measurements in the model tests were the 6 degrees of freedom (D.O.F.s) rigid body motions, mooring line tensions, and the forces between the spar and torus in 3 directions (X, Y and Z). The wind speed was also measured by a sensor in front of the model and the wind force on the wind turbine disk was measured by a load cell installed on top of the tower. This paper describes the model test set-up for the two survival modes, the test results and the numerical model. The results from the entire test matrix of model tests and numerical simulations are presented and compared. The numerical results agree well with the test results for the survival mode with the WEC fully submerged for which the linear hydrodynamic loads dominate. In addition, several nonlinear phenomena were observed during the tests, such as wave slamming, Mathieu instability and vortex induced motion. These nonlinear phenomena were not captured by the present numerical model and the work on a refined hydrodynamic model is still ongoing.

Key words: Spar Torus Combination; Combined Wind and Wave Energy Converter Concept; Model Test; Survival Mode; Numerical model; Uncertainty Analysis.

## 2 Introduction

Wind energy is becoming an increasingly important source of renewable energy. By June 2014, about 337 GW wind power generation capacity has been setup in the world (The World Wind Energy Association, 2014). The installed offshore capacity in Europe has reached more than 8 GW by the end of 2014 (The European Wind Energy Association, 2015). Offshore wind technology has been rapidly developed in recent years with a trend towards larger scale wind turbines, increased water depth, with sites further from shore and larger wind farm size. Large scale wind turbines such as the National Renewable Energy Laboratory (NREL) 5 MW reference wind turbine (Jonkman et al., 2009) and the DTU 10 MW reference wind turbine (Bak et al., 2013), have been designed and are being used in comparative studies by several research groups. The support structures for the offshore wind turbines are mostly bottom-fixed so far, but there are increasing interest in developing floating wind turbines. Several model tests for floating wind turbines have been performed: model tests on concepts with the NREL 5 MW wind turbine atop three generic floating platforms, i.e., spar, tension leg and semi-submersible (Goupee et al., 2012; Jonkman, 2010) at a 1:50 scaling ratio have been tested in Maritime Research Institute Netherlands (MARIN). Some prototypes have also been tested: Hywind with a 2.3 MW wind turbine was launched in 2009 (Stiesdal, 2009); WindFloat with a 2MW wind turbine was installed in 2011 (Principle Power Website, 2015); and two floating wind turbines were installed in Japan in late 2013, a semi-submersible with 2 MW downwind turbine (Fukushima Offshore Wind Consortium, 2013) and a spar with a 2 MW wind turbine (GOTO FOWT Website, 2015).

Wave energy also represents an energy resource with a large potential and with a much higher power density than wind power. The worldwide overall resource which is around 2 TW is of the same order of magnitude as the world's electricity consumption (Cruz, 2008). The research on wave energy was intensified during 1970s and was spurred by the famous cam-shaped floating body known as Salter duck developed by (Salter et al., 2002). Up to now, many offshore Wave

* Corresponding author. Tel: +47 47448557; Fax: +47 73595528
E-mail address: ling.wan@ntnu.no (Ling Wan)

Energy Converters (WECs) concepts or prototypes have been built or proposed, they can generally be categorized as oscillating bodies, oscillating water column, overtopping device (Falcão, 2010).

Commercial wind or wave farms usually occupy large ocean spaces. For this reason, combining the wind and wave energy converters in the farm configurations would be beneficial for the utilizing the space and energy. In the view of investment reduction, it would also be beneficial for the wind and wave energy converters to share the infrastructures such as support structure, power substations, mooring system and cables. The EU FP7 Marine Renewable Integrated Application Platform project (MARINA Website, 2015) is one of such projects that addresses the integration of wind and wave energy devices on a single platform with focus on floating concepts for deep water application. Several combined wind and wave energy converter concepts have been proposed through this project, with a focus on the spar-torus combination (STC) concept; the semi-submersible flap concept (SFC) and the oscillating water column (OWC) array with a wind turbine installed. The SFC (Luan et al., 2014; Michailides et al., 2014) uses a 5 MW semi-submersible floating wind turbine with three flap-type WECs that are installed on the three pontoons. Functionality and survivability tests of the SFC with a 1:50 scale ratio have been performed in the ocean basin at Ecole Centrale De Nantes (ECN), France. The OWC array platform has been proposed by the Hydraulics and Maritime Research Centre in University College Cork (HMRC/UCC). The OWC arrays include 20 OWC chambers with 10 OWCs installed in each arm facing the main wave direction, and a wind turbine is installed on top of the structure. The STC concept is the focus in this paper.

The STC concept (Muliawan et al., 2012), which is shown in Figure 1, combines a spar floating wind turbine and a torus-shaped heaving body wave energy converter. The wind turbine installed in the STC is the NREL 5MW reference turbine, while the WEC in the STC is inspired by the WaveBob (WaveBob, 2014) concept, which was developed between 1999 and 2013. In the STC concept, the torus WEC can move along the cylinder of the spar to absorb the wave energy. Rollers and mechanical brake system are installed between the spar and the torus. The roller can allow the relative heave motion between the two bodies and restrict the relative horizontal motion between them for operational conditions, while the mechanical brake can restrict the relative heave motion, and keep the two bodies moving together for survival conditions. An end stop system is also incorporated to limit the excessive relative heave motion under operational conditions. The end stop system, roller and mechanical brake system are shown in Figure 1. The wind turbine and WEC can share the same floater, cables and mooring systems. The offshore site considered for design is located 30 km from the west coast of Norway (Li et al., 2013).

Numerical simulations (Muliawan et al., 2013b) have shown a positive synergy between the two bodies under operational sea states. However, under extreme conditions, the structure is subjected to severe wind and wave loads. Under extreme conditions, the rotor of the FWT can be parked, and the blade can be feathered into the wind to reduce the wind loads. The heave natural period of the WEC in the STC is around 6s with no damping applied, but in operational condition with power take off (PTO) damping applied, the natural period of the STC will increase from 6 s to 13 s, which coincides with the periods of waves with significant energy. Considering the large water plane area of the torus as compared to that of the spar and the natural period which is close to the main wave periods under extreme conditions, the structure will experience significant responses in severe waves due to resonance. Several alternative survival modes have been considered for the STC concept (Muliawan et al., 2013a):

- Mode I: the WEC PTO system is released, the wind turbine is parked, and the torus moves freely along the spar. The motion is only limited by the end stop system. This is referred to as the released survival mode. This mode will result in extremely large end stop forces and is not considered to be a viable solution, so it will not be discussed further here.
- Mode II: the WEC PTO system is released, the wind turbine is parked, and the torus is locked mechanically to the spar at the mean water level (MWL). In this mode, the two bodies are locked and can move together. This is referred to as the MWL mode hereafter.
- Mode III: the WEC PTO system is released, the wind turbine is parked, and the torus is locked mechanically to the spar. By adding ballast to the torus or the bottom of the spar, the two bodies are submerged to a specified position. In this mode, the torus is totally submerged (SUB) in the water. This mode is referred to as the SUB mode hereafter.

The three survival modes are shown in Figure 1:

## 3 STC model and test facility

Model tests for the survivability of the STC were performed in the towing tank of MARINTEK, Norway. The tests were carried out to validate the numerical model and to investigate the performance of the STC survival modes under extreme conditions. The MWL and SUB modes were the focus for investigating possible strategies for survivability (Wan et al., 2014). The measurements from the model tests were the motions, mooring forces and interface forces between the spar and the torus.

In the model test, geometrical similarity, kinematic similarity and dynamic similarity need to be satisfied. If the Froude number $Fn=U/(gL)^{0.5}$, is kept the same between the full scale and model scale structures, the Froude scaling is followed, which ensures the ratio of the inertia and gravity forces the same between the model scale structure and the prototype. In the Froude number, U is the characteristic velocity, g is the gravitational acceleration and L is the characteristic length of the model. The STC model was downscaled by Froude scaling with a ratio of 1:50. The scaling factors for the different variables are listed in Table 1. For extreme sea states, there are usually large H/D and small $\pi D/L$ applied, where H is the wave height, D is the characteristic dimension and L is wave length. For the STC, D=20 m for the torus and 6.45 m for the spar, assuming H=30 m, then H/D<5, drag may become relatively important as compared to smaller waves.

The dimensions of the STC model are shown in Table 2, the drafts for the different survival modes are listed in Table 3, and the weights are listed in Table 4. All of the values in this paper are presented at the full scale unless otherwise specified. The simulation model is at the model scale, but the results are up-scaled to the prototype scale. The model test results were also up-scaled. In the SUB mode, the whole model was submerged by 26 m compared with the MWL mode. In this case, the distance from the bottom of the torus to the still water line (SWL) would be 30 m in the SUB mode, compared to the torus draft of 4 m in the MWL mode. This draft change can be modified in the prototype by changing the ballast.

The model test facility and layout are shown in Figure 2. The towing tank is 260 m long, 10.5 m wide and with two different depths of 10 m and 5.6 m. The depth is 10 m from the wave maker over a 85m distance, and is 5.6 m in the other part of the tank (MARINTEK, 2014). The maximum wave height and wave period range can be generated by the wave maker is 0.9 m and 0.8 – 5 s respectively in model scale. The model is placed in the position with 10 m water depth. The coordinate system of the model test is set as follows: the z direction is positive downward, and the x direction is positive in the wave maker direction. The origin is assumed to be at the intersection of the still water surface and the central line of the cylinder. Four resistance-type wave probes were used in the tests. The first is located 15.5 m in positive x direction, the second and fourth are located 2 m in the positive and negative x direction, respectively, and the third is located 0.77 m in the positive x and 2.67 m in the negative y direction. Two rows of fans with four fans in each row are installed in front of the model to generate wind. To reduce the lateral mean wind speed and the occurrence of large turbulent eddies, honeycomb structures were used. The wind generated can be assumed constant along the vertical direction. The wind velocity sensor was installed between the fans and the STC model. All the control and electronic devices, e.g., computers for recording data, controlling the wave maker, wind generation, carriage position, and cameras, as well as the A/D converters, channel amplifiers and so on are all located on the control platform. Pictures of the test facilities are shown in Figure 3.

The STC model is shown in Figure 5, each part of the model and the material used are illustrated. The coordinate system is also shown. The still water levels for the MWL and SUB modes are shown with blue lines in Figure 5 and Figure 6.The tower and main buoyant part of the floater are composed of PVC material, and the cylinder in the middle part of the model (i.e., the upper part of the spar floater) is composed of aluminum alloy. The aluminum alloy has a low weight but high stiffness that allows the installation of load cells between the two bodies. The torus is made of two materials: the core is composed of Dyvincell, and aluminum alloy plates are located on the top and bottom of the core.

Eighteen HBM DF-2S water-proof bending load cells were combined and installed to measure the forces between the spar and torus as shown in Figure 6. These load cells rigidly connected the two bodies and measured the total forces and moments in the global x, y and z directions. The eighteen load cells were installed at six positions and for each position, there were three load cells combined. Three of the positions were located on the top of the torus and they were 120 degrees apart with respect to the vertical axis of the cylinder; the other three positions were located on the bottom of the torus with the same x and y coordinates of the top ones. At each position, three load cells were combined orthogonally to measure the forces in three local directions. The total forces along the three global directions were then calculated from these load cell measurements. For each load cell, the measured force was assumed to be applied on the center of the load cell, and then the moment could be derived by knowing the distance of the force applied position to the origin of the coordinate system for MWL mode. For a single load cell, the nonlinearity, the hysteresis error and the creep over 5 mins are all between -0.05% to +0.05% of the sensitivity.

The catenary delta line mooring system was deployed in the prototype as shown in Figure 1. The mooring line tension was provided by the mooring line weight in water and the catenary line geometry. To limit the yaw motion of the prototype, a delta shape mooring configuration in each fairlead part was deployed. In the model test, the mooring system was simplified as 3 rigid bars connected by 3 linear springs. This configuration can provide yaw stiffness as the delta mooring configuration in the prototype.

The motions of the model were recorded using the Qualisys system and were tracked by 3 reflection balls and 8 cameras. The reflection balls are installed on top of the tower as shown in Figure 5. By hammering test, the tower first and second flexible mode is around 7 Hz and 19 Hz in model scale, which is much higher than the wave frequency range (around 0.3 Hz – 1 Hz) and horizontal mooring stiffness of the model which is around 0.07 Hz. Hence, the tower is rigid enough.

The wind tests were performed to model the correct mean wind thrust or drag forces on the turbine. The wind thrust curve is shown in Figure 4. The wind power is not considered. After cutout wind speed 25 m/s, the wind turbine will be parked and the blades will be feathered to the wind, so there is only wind drag on the blade, and there is no centrifugal force, and gyro moment. At rated wind speed of 11.4 m/s, the thrust force on the rotor reached the maximum value. Two disks of different diameters were used to model the two different thrust forces based on the drag formulation on the flat plate: $F = 0.5\rho A C_d V^2$, where $F$ is the thrust force on the disk; $A$ is the disk area; $C_d$ is the drag coefficient, which is assumed to be 1.9 according to the DNV rule (DNV, 2010); ρ is the density of the air; and V is the relative wind velocity. In the test, the wind velocity and wind thrust were both downscaled by Froude scaling. The diameter of the disk can be calculated based on the prototype thrust curve and the designed wind velocity. The diameter of the large disk is 185 cm, and the diameter of the small disk is 15 cm. The small disk is used to model the thrust force under extreme wind conditions, and the large disk is used to model the thrust force under operational conditions. The centrifugal forces, rotation moment and aerodynamic damping and so on were not taken into account. It should be noted that, in the operational sea states tested, the STC was still in the survival conditions, i.e., the MWL and SUB modes. The wind probe was installed between the fans and model at a height of approximately 75 m above the MWL.

## 4 Test matrix

The test procedure is described below.  The test procedure applied to both the MWL and the SUB mode.

First, hammering tests were performed before and after putting the model in the water by hitting the model with a hammer at several locations on the spar or torus. The main purpose of the hammering tests was to identify the eigen frequencies of the torus local vibration, and the torus global vibration with respect to the spar in the 6 degrees of freedom (D.O.F.s). Such mode would be excited when the bottom slamming occurs for the MWL mode in large waves.

Second, decay tests were performed for the 6 D.O.F.s of the rigid body motions. The natural periods and damping levels can be determined from the measured decay curves.

Third, regular wave tests were performed to determine the transfer functions of various response parameters, such as the motions, interface forces between the spar and torus, and mooring tensions. The wave periods varied from 7s to 23s, and two sets of wave heights were tested with H=2 m and H=9 m. For H=2 m, the waves are mostly linear waves, while for H=9 m, the waves vary from linear waves to the 5$^{th}$ order Stokes waves (DNV, 2010). For H=9 m, the viscous effect should be important as compared to H=2 m. In the numerical model, linear wave theory is assumed.

Fourth, tests in irregular waves with no wind were considered. Three sea states were selected based on the metaocean data of the western coast of Norway. For extreme sea states, an IFORM method (Winterstein et al., 1993) was used to establish the 3D 50-year contour surfaces of Uw (mean wind speed at 10m height), Hs and Tp for the selected sites, and then a condition with maximum Uw and a condition with maximum Hs are selected as the extreme sea states. At last, one operational sea state (Hs=2.75 m, Tp=11 s) and two extreme sea states (Hs=13.5 m, Tp=15 s and Hs=15.3 m, Tp=15.5 s) were chosen as the testing sea states. All of the generated waves follow the Joint North Sea Wave Observation Project (JONSWAP) spectrum, which covered the energy between 5 s to 30 s in full scale, and several tests were performed for each sea state using different seeds.

Fifth, wind only tests and combined irregular wave/wind tests were performed. Based on the irregular wave tests, wind condition was considered, with the Uw=33.3 m/s for extreme sea state of Hs=13.5 m, Tp=15 s, and Uw=31.4 m/s for extreme sea state of Hs=15.3 m, Tp=15.5 s. For the operational sea state, a wind velocity of 11.4 m/s was selected. Only constant and uniform wind fields were used for the combined irregular wave/wind tests. First, the wind only tests were performed to investigate the wind effects without waves. Then, the wave was incorporated and the wave conditions were the same as those in the pure irregular wave tests. For the tests with wind, the large wind disk was used for operational wind conditions, and the small disk was used for extreme wind conditions. In the two extreme sea states, two mean wind velocity with very small difference in model scale was required, but due to the step voltage control of the wind generating system and the open space condition, it was difficult to generate the desired mean wind speeds with high accuracy so finally the same mean wind speed of 38 m/s in full scale was generated for the two extreme sea states.

## 5 Numerical modelling

To simulate the complex system including the spar, the torus and their coupling effect as well as the mooring system and wind loads, an integrated analysis is needed. A nonlinear model including the viscous Morison drag and quadratic damping terms to predict the motion and force responses are included. In this case, a frequency domain model is not applicable. The simulations in this paper are based on the hybrid frequency- and time-domain model (Naess and Moan, 2013) in model scale.

The hydrodynamic properties of the test model, i.e., the linear excitation forces for each body in the 6 D.O.F.s, added mass, potential damping and coupling terms of the two bodies are calculated in the frequency domain using the software Sesam/Wadam (DNV, 2011). The frequency domain motion equation can be expressed as:

$$-\omega^2\big(\mathbf{M}+\mathbf{A}(\omega)\big)\mathbf{x}(\omega)+\mathrm{i}\omega\mathbf{C}(\omega)\mathbf{x}(\omega)+\mathbf{R}\mathbf{x}(\omega)=\mathbf{F}(\omega) \tag{1}$$

in which $\mathbf{M}$ is the structural mass matrix; $\mathbf{A}(\omega)$ is the frequency domain added mass matrix; $\mathbf{x}(\omega)$ is the frequency domain displacement; $\mathbf{C}(\omega)$ is the potential damping coefficients matrix; $\mathrm{R}$ is the restoring coefficient matrix; and $\mathbf{F}(\omega)$ is the external force. Equation 1 is based on linear potential theory. If some nonlinear effects should be incorporated, a time domain model is needed. The equation of motion for a rigid floating body considering the quadratic viscous damping with 6 D.O.F.s can be written in the time domain as:

$$\big(\mathbf{M}+\mathbf{A}(\infty)\big)\ddot{\mathbf{x}}(\mathrm{t})+\mathbf{B}\dot{\mathbf{x}}|\dot{\mathbf{x}}|+\int_0^{\mathrm{t}}\mathbf{k}(\mathrm{t}-\tau)\,\mathbf{x}(\tau)\mathrm{d}\tau+\mathbf{R}\mathbf{x}(\mathrm{t})=\mathbf{f}(\mathrm{t},\mathrm{x},\dot{\mathrm{x}}) \tag{2}$$

in which $\mathbf{A}(\infty)$ is the added mass matrix at infinite frequency; $\mathbf{x}$, $\dot{\mathbf{x}}$ and $\ddot{\mathbf{x}}$ are the displacement, velocity and acceleration in time domain, respectively; $\mathbf{B}$ is the quadratic viscous damping coefficients matrix; $\mathbf{k}(\tau)$ is the retardation function, which is based on the added mass and potential damping matrix; and $\mathbf{f}(\mathrm{t},\mathrm{x},\dot{\mathrm{x}})$ is the summation of the external force in time domain related to the displacement and velocity.

The motion equation in the STC model has 12 D.O.F.s due to the two-body model. The excitation forces in the simulation include the Froude-Kryloff forces and diffraction forces, which are calculated using the 1st order potential flow theory by the panel method, while the drag force is simulated by a series of slender elements with specified Cd values according to Morison's equation. The wind thrust force is simulated by the drag force on the disk, and it is calculated based on the measured wind velocity and the disk area. The wind drag force on the tower is modelled by a clump force applied at the middle point of the tower above the still water plane. The mechanical couplings are modeled as linear spring-damper systems. Due to the mechanical coupling, a small time step is used in the time domain calculation. The mooring system is modeled by linear springs. The time domain model is modelled and solved in Simulation of Marine Operation (SIMO) (MARINTEK, 2007), which was developed by MARINTEK. The motion equation for the STC model can be expanded and rewritten based on equation 2 as:

$$\begin{bmatrix}\big(\mathbf{M}+\mathbf{A}(\infty)\big)_{11} & \mathbf{A}(\infty)_{12}\\ \mathbf{A}(\infty)_{21} & \big(\mathbf{M}+\mathbf{A}(\infty)\big)_{22}\end{bmatrix}\begin{bmatrix}\ddot{\mathbf{x}}_1(\mathrm{t})\\ \ddot{\mathbf{x}}_2(\mathrm{t})\end{bmatrix}+\begin{bmatrix}(\mathbf{B})_{11} & \mathbf{0}\\ \mathbf{0} & (\mathbf{B})_{22}\end{bmatrix}\begin{bmatrix}\dot{\mathbf{x}}_1(\mathrm{t})|\dot{\mathbf{x}}_1(\mathrm{t})|\\ \dot{\mathbf{x}}_2(\mathrm{t})|\dot{\mathbf{x}}_2(\mathrm{t})|\end{bmatrix}+\int_0^{\mathrm{t}}\begin{bmatrix}\mathbf{k}_{11}(\mathrm{t}-\tau) & \mathbf{k}_{12}(\mathrm{t}-\tau)\\ \mathbf{k}_{21}(\mathrm{t}-\tau) & \mathbf{h}_{22}(\mathrm{t}-\tau)\end{bmatrix}\begin{bmatrix}\dot{\mathbf{x}}_1(\tau)\\ \dot{\mathbf{x}}_2(\tau)\end{bmatrix}\mathrm{d}\tau$$

$$+\begin{bmatrix}(\mathbf{R})_{11} & \mathbf{0}\\ \mathbf{0} & (\mathbf{R})_{22}\end{bmatrix}\begin{bmatrix}\mathbf{x}_1(\mathrm{t})\\ \mathbf{x}_2(\mathrm{t})\end{bmatrix}=\begin{bmatrix}\mathbf{f}^{\mathrm{wind}}(\mathrm{t})\\ \mathbf{0}\end{bmatrix}+\begin{bmatrix}\mathbf{f}^1{}_1(\mathrm{t})\\ \mathbf{f}^1{}_2(\mathrm{t})\end{bmatrix}+\begin{bmatrix}\mathbf{f}^2{}_1(\mathrm{t})\\ \mathbf{f}^2{}_2(\mathrm{t})\end{bmatrix}+\begin{bmatrix}\mathbf{f}^{\mathrm{drag}}{}_1(\mathrm{t})\\ \mathbf{f}^{\mathrm{drag}}{}_2(\mathrm{t})\end{bmatrix}+\begin{bmatrix}\mathbf{f}^{\mathrm{coupling}}{}_1(\mathrm{t})\\ \mathbf{f}^{\mathrm{coupling}}{}_2(\mathrm{t})\end{bmatrix} \tag{3}$$

in which the subscript 1 or 11 signifies the variables of body 1 (spar); subscript 2 or 22 signifies the variables of body 2 (torus); subscript 12 or 21 signifies the coupling terms between the spar and the torus. The vertical (heave) quadratic damping of the spar and torus are modelled by the quadratic damping matrix on the left side of equation 3, while the horizontal drags are modelled by Morison drag forces and are signified by the drag term on the right side; $\mathbf{f}^{\mathrm{wind}}(\mathrm{t})$ is the wind drag on the tower and disk; $\mathbf{f}^1{}_1(\mathrm{t})$ and $\mathbf{f}^2{}_1(\mathrm{t})$ are the 1st and 2nd order wave forces applied on the spar, respectively; $\mathbf{f}^{\mathrm{drag}}{}_1(\mathrm{t})$ and $\mathbf{f}^{\mathrm{drag}}{}_2(\mathrm{t})$ are the total Morison drag forces on the spar and torus, respectively; the interface forces between the two bodies can be expressed as $\mathbf{f}^{\mathrm{coupling}}{}_1=\mathbf{R}'\big(\mathbf{x}_1(\mathrm{t})-\mathbf{x}_2(\mathrm{t})\big)+\mathbf{B}'(\dot{\mathbf{x}}_1(\mathrm{t})-\dot{\mathbf{x}}_2(\mathrm{t}))$, where $\mathbf{R}'$ and $\mathbf{B}'$ are the stiffness and damping coefficients matrix of the load cells, respectively, and $\mathbf{f}^{\mathrm{coupling}}{}_1=-\mathbf{f}^{\mathrm{couple}}{}_2$.

Considering the long cylindrical body of and the Re number which is smaller than $1\times10^5$, the flow in the horizontal plane is in subcritical flow region (DNV, 2010). During the numerical simulations, the quadratic coefficient Cd=1.2 in Morison's formula is used for the horizontal direction, and Cd=1.9 is used for the vertical direction, where sharp corners exist. In addition, the wave forces and drag forces on the delta mooring bars are also taken into account by assuming Cd=1.2. These drag coefficients were chosen based on the estimated Reynolds number and the structural shape of the model. Due to the complex shape of the model, the selection of Cd can be empirical, so other Cd values were also considered to evaluate the uncertainties.

To account for the 2nd order effect in the STC, Newman's approximation (Faltinsen, 1993) is used to estimate the slow-drift motions. The mean drift forces are calculated based on the pressure integration method, and the low frequency part of the wave force spectrum is calculated by SIMO based on the input sea state spectrum according to Pinkster's formula (Pinkster, 1975) as:

$$S_F(\mu) = 8\int_0^\infty S(\omega)S(\omega+\mu)\left(\frac{\bar{F}_i(\omega+\mu/2)}{\zeta_a^2}\right)^2 d\omega \qquad (4)$$

where $\bar{F}_i(\omega+\mu/2)$ is the mean wave load in direction $i$ for frequency $\omega+\mu/2$; $S(\omega)$ and $S(\omega+\mu)$ are the wave spectral values for the frequencies $\omega$ and $\omega+\mu$, respectively; $\zeta_a$ is the incoming wave's amplitude; and $\bar{F}_i(\omega+\mu/2)/\zeta_a^2$ is the mean drift force transfer function. The second order forces for the STC were calculated by considering the model as one body, and the forces were applied on the spar in the SUB mode and on the torus in the MWL mode.

## 6 Comparison of test and numerical results

The test results for the SUB and MWL survival modes are presented and compared with the numerical results in this section.

### 6.1 Decay tests and the comparison with simulations

The 6 D.O.F.s decay tests were performed, and the natural periods of the rigid body motion and damping ratios are presented in Table 5 for both the MWL mode and the SUB mode. The yaw motion decayed rapidly due to the supercritical damping level, so the natural period and damping level of the yaw were not identified. In the MWL mode, the roll and pitch decays were strongly coupled with the surge and sway motions, so the pitch and roll damping ratios were not identified clearly. The numerical results agree very well with the test results.

### 6.2 Regular wave tests and the comparison with simulations

Regular wave tests were performed to determine the transfer functions between the responses and the incident waves as well as possible nonlinear effects due to large waves. The results show the responses to sinusoidal waves for different wave periods and wave heights. Several wave periods and two wave heights were tested for each survival mode. The small wave height is 2 m, and the large wave height is 9 m. Note that strongly nonlinear phenomena were observed during the regular wave tests. Slamming and green water as well as Mathieu type instability were observed for the MWL mode. The vortex induced motion (VIM) was observed for the SUB mode. The regular wave test matrix and the occurrence of nonlinear phenomenon are shown in Table 6, where the cases for the nonlinear phenomena are with colored background.

'Slamming' (Faltinsen, 1993) often refers to impulse loads with high pressure peaks that occur during impacts between the body and water and represent local liquid-structure impacts. Slamming is dangerous for the WEC and the interface between the torus and spar because the impact will induce large loads, which depend on the local relative structure-fluid velocity and the local geometry in the impact region (dead-rise angle). When the torus and the spar are locked together, the heave natural period of the STC is 12.7 s, which is located in the frequent wave period region. Moreover, due to the small draft of the torus (4 m), water exit and entry phenomena of the torus are expected to occur. Under small wave heights (H=2 m), water exit was observed only for waves with the periods close to the heave natural period, i.e., approximately T=12 s and T=13 s. However, due to the small draft and height of the torus, slamming and green water can be observed with the large wave height (H=9 m) for most of the wave periods.

Mathieu-type instability (Haslum and Faltinsen, 1999; Koo et al., 2004) is a kind of instability that occurs when the wave excitation period is half of the pitch natural period, the pitch resonance is exited. This is due to the influence of the heave motion on the pitch restoring term, which becomes time varying. This instability was observed for T=17 s and 19 s, which represent relatively long waves. In these cases, the period for pitch motions evolves gradually from the wave period to twice the wave period, while the pitch amplitude also increases to a constant value.

For the SUB mode, the VIM was observed. The VIM usually happens when there is current passes a cylinder, and the vortex shedding frequency is close to the resonant frequency of the motion and causes the resonance. In the tests, the transverse motions (sway and roll) and the yaw motion increased gradually for large wave periods of T=23 s and T=25 s. The nonlinear phenomena observed during the test will not be discussed in this paper due to the lack of space.

The steady-state response amplitude of every channel was divided by the input wave amplitude to obtain the Response Amplitude Operator (RAO) in the numerical simulations. To obtain the test results, the RAO was calculated by dividing one cycle of the steady-state model response by the corresponding wave height at the model position. Even in the steady state of the regular wave test, due to the variations of the input to the wave maker, the wave height is not exactly the same but varies slowly with a small change in amplitude, so the response also varies. In this case, the scatter of the RAO based on 20 wave cycles was investigated. The standard deviation (STD) is shown as the error bars in Figure 7 and Figure 8.

For the SUB mode, the numerical results were considered for the two wave heights. The RAO of each channel for the SUB mode and a comparison with the test results are plotted in Figure 7. The RAOs for large waves are smaller than those for small waves due to the significant effect of damping near the resonant period.

In the regular wave tests for the MWL mode, there is no strong nonlinear effect for small waves. The RAOs from the tests and simulations considering only small waves are plotted in Figure 8. The comparisons show a small inconsistency in the resonant area (approximately T=13 s), where nonlinear phenomena water exit and entry occur. Regular wave tests were also performed for the large wave height (H=9 m), but strong nonlinear phenomena were observed. The heave resonant motions at the natural period of 13 s were excited for the MWL mode, and the vertical force RAO follows the heave RAO. For the STC, the surge is partly induced by the pitch, and they generally follow a straight line in RAO results because the resonant period is away from the wave period.

For both the SUB and the MWL modes, large discrepancies of the RAO comparisons for mooring line tension appear. The mooring line 1 tensions are the most significantly underestimated by the numerical simulations. This is because the relatively large-size springs were used for the mooring lines in this test and the mass of the mooring line 1 is approximately 4 times greater than the mass of mooring 2 or mooring 3. The mass of the springs were not taken into account in the numerical simulations in SIMO, i.e., the inertia effect of the mooring springs was not considered.

Figure 9 shows the configuration of the mooring spring system in the test, in which one end of mooring spring 1 was connected to the mooring bar and the other was connected by a rope to a steel bar that was fixed to the carriage, while mooring lines 2 and 3 were connected by ropes to the side walls of the tank. Mooring line 1 was modeled by 4 springs that were series-parallel connected, while mooring lines 2 and 3 each have only one spring. Thus, the mass of mooring line 1, which was approximately 1.5 kg in model scale, was approximately 4 times that of mooring 2 or 3. In addition, the rope for mooring line 1 was quite long. Because of the large weight and the length of the rope, mooring spring 1 was curved under static conditions, which caused problems in measuring the mooring forces, as shown in the left figure of Figure 9. One problem was that the measured force includes the dynamic effect of the mooring springs; another was that the measured force was not exactly horizontal but it was inclined.

During the tests, the spring 1 not only provided stiffness. There also exists wave excitation loads on the spring as well as the inertia effect of the spring, which induce dynamic loads on the floater in addition to the restoring forces. As dynamic excitation forces, the mooring line 1 force RAO and the excitation force RAOs of the spar and the torus in surge (F1) and heave (F3) directions in the MWL mode are compared in the right figure of Figure 9. In 12 s and 13 s, there was slamming observed, so the mooring line forces will not be linear. The percentage of mooring line 1 force RAO in non-slamming region compared with the F1 force RAO for the spar is from 0.7% in 21 s to 7.3% in 14 s, with the mean percentage of 2.8%. Considering the linear relationship between motion and external forces by different excitation components in each wave frequency, the mean discrepancies on motions caused by the dynamic mooring forces is under 2.8%. Considering the incline of the mooring line 1, the horizontal tension is smaller than the measured mooring line tension, which makes the discrepancies even smaller. So it can be concluded that the effect of the mooring dynamic effect to the motion of the STC is limited. However, the dynamic effect is important to consider when looking at the mooring line tension. The mooring dynamic effect will be further discussed in the uncertainty part of this paper.

## 6.3 Irregular waves and wind conditions

The test matrix for irregular waves and wind is shown in Table 7. There are irregular wave only tests, wind only tests and the irregular wave+wind tests for both the MWL mode and the SUB mode. Only constant and uniform wind speed was considered. The response of the STC with irregular waves was tested in one operational sea state and two extreme sea states. Realizations with different seeds were carried out for each sea state, and the number of realizations is shown in Table 7. The recorded effective time for each test was more than 1.5 hours at the full scale.

For the wind cases, the large wind disk was used for the operational wind conditions, and the small disk was used for the extreme wind conditions to model the correct thrust force. The wave conditions in the wave+wind tests were the same as those used in the wave only tests. Cases A1 to A3 refer to the irregular wave only tests, B1 and B2 refer to the wind only tests, and C1 to C3 refer to the irregular wave only plus wind tests.

All of the generated waves followed the 3-parameter JONSWAP spectrum with the given Hs, Tp and peakedness parameter $\gamma$. The higher is the $\gamma$ value, the sharper is the JONSWAP spectrum shape. For the two selected extreme sea state, $\gamma$=3 is suggested by (DNV, 2010). For the operational sea state, $\gamma$=1 is suggested. The measured wave spectrum and input wave spectrum are compared in Figure 10. In addition, the statistical property of the generated waves are investigated, and the probability distribution function (PDF) and cumulative distribution function (CDF) are shown in Figure 11 and compared with the Gaussian distribution.

## 6.4 Irregular wave tests and the comparison with simulations for the SUB mode

The numerical simulation time series and spectral results for the SUB mode in A1 are compared with the test results in Figure 12. The simulation model considered the 1st and 2nd order wave forces. The resonant frequencies are 0.061 rad/s for surge, 0.134 rad/s for heave, and 0.242 rad/s for pitch. The simulation response time series agree well with the test results; both the amplitudes and phases show good agreements. Large wave-frequency motion responses and small low-frequency motion responses in surge and pitch are observed in the test and simulations. There is no wave energy at 0.134 rad/s. But there is significant response in heave, due to the second-order wave loads. The slow drift motions in surge and pitch are also observed in the simulation that considers only the 1st order wave potential and this is due to the quadratic viscous effect by the drag element forces around the instantaneous free surface that gives a 2nd order effect. But, the magnitude is smaller than that obtained from the test. The 1st order simulation failed to predict the slow drift for heave, while the 2nd order model captured this effect. There are no observable low-frequency responses in the interface forces in x direction (FX) and z direction (FZ).

Figure 13 compares the responses from the tests, the simulations based on the 1st order wave forces and simulations based on the 2nd order wave forces in the extreme sea state A3. The responses properties under sea state A3 is similar to that under A1. Comparisons of the response time series and spectra are presented. The time domain comparison shows good consistency between the tests and simulations, and the frequency domain plot shows good consistency in the wave frequencies. However, in the low frequency part, the surge and heave motions are slightly underestimated by the simulations. The time and frequency domain comparisons of the interface forces are also presented and show that the 2nd order wave force has a negligible effect on the force channels.

Figure 14 plots the mooring line force spectrum from the tests and simulations based on the 1st order and 2nd order wave force for sea state A3. In the test results, there are significant peaks in the resonant frequencies of surge and pitch. There are also obvious responses in the wave range for the mooring spectrum of the tests, especially for mooring spring 1. In the simulation, the slowly varying responses in surge and pitch resonant frequencies dominates the mooring line tensions, while the mooring line tension responses in wave frequency is insignificant. The reason for the large wave frequency responses in the mooring line 1 for the tests is due to the mooring dynamic effect mentioned above.

## 6.5 Irregular wave tests and the comparison with simulations for the MWL mode

Irregular wave tests were also performed for the MWL mode, and the cases are shown in Table 7. In cases A1 and C1 (operational sea states), little slamming occurred. In cases A2, A3 and C3 (extreme sea states), the excitations were so large that water exist and entry problems were observed and very large slamming forces were measured. This section of the paper presents the simulation results and compares them with the test results. However, the current numerical model doesn't include the slamming force.

The resonant frequency is 0.064 rad/s for the surge, 0.174 rad/s for the pitch and 0.483 rad/s for the heave under the MWL mode. Plots of the test results, the simulation results considering only the 1st order wave loads and the simulation results considering the 1st and 2nd order wave loads for case A1 are shown in Figure 15 and Figure 16. In the simulations, the 1st plus 2nd order model gives good results compared to the tests; however, the 1st order model failed to capture the large slow-drift motion. The WEC has a large water plane area, which reflects large waves, so 2nd order force should be larger (as compared to the SUB mode) according to Maruo's formula (MAURO, 1960) considering that the WEC is locked on the spar and no wave power was absorbed.

In the MWL mode, the heave natural period was in the wave region and the resonant heave motion was excited, but because the excitation was small in the operational sea state, there were few slamming problems. In the surge and pitch response spectra, there are two clear peaks which correspond to the natural frequencies in surge and pitch. In the interface force spectra, the peaks are mostly in the wave frequency region, and the low frequency part is not as significant as in the motion spectra. For the mooring force spectrum, mooring line 1 has a large value in the wave frequency region, which is the same as in the SUB mode.

In extreme sea states A2, A3, C2 and C3, the resonant heave motion was large, and strong nonlinear phenomena were present, such as slamming and green water. The simulation cannot capture these phenomena. However, the comparisons between the simulation results and test results are still presented to investigate the difference. Due to the large heave motion in the extreme sea states, the WEC continually exited and entered the water, which induced large water impact forces. The slamming and green water together with the change of buoyancy force had effects on the motion responses. The results for the motion responses are shown in Figure 17. Figure 18 shows the force response results. The test results in Figure 17 show that the slow drift motion is still dominant but is not as significant as that in the operational sea states and that due to the exit and entry from the water, the motions are reduced compared with the motions without slamming, as shown in the simulation results. This process can be described as follows: when the WEC goes out of the water, there will be suction force on the WEC bottom. And then, both the hydrostatic and hydrodynamic forces will disappear. Only the gravity force and the inertial force will act on the STC. While, when the WEC re-enters the water, there is significant slamming force in addition to the normal hydrostatic and hydrodynamic forces. When the WEC is fully submerged, the WEC top surface also becomes wet and there will be additional hydrostatic and hydrodynamic pressure loads on this surface.

Figure 18 shows clear force peaks due to the impact of the water, and the impact forces are very high frequency components with high values (not shown in the spectral plot), which are critical to the ultimate strength and fatigue damage to the structure. The spectrum plot also shows that the simulation gives significantly higher values in the low frequency range of Fx and over predicts the values in the wave frequency range.

Further investigation on the water exit and entry problems is needed.

## 6.6 Wind tests and the comparison with simulations

In the prototype under extreme conditions, the turbine is parked, and the blade is feathered to reduce the wind load. The wind thrust curve shows that the wind thrust on the rotor is greater under operational cases than under extreme conditions. In extreme test cases, the absolute mean wind velocity is approximately 38 m/s, and the turbulence intensity measured is approximately 0.3, which is high in offshore conditions.

In this model test, no intention to study the behavior of the STC under turbulent wind was made. Only constant and uniform wind conditions were considered. The main purpose to consider wind conditions is to study its effect on the motions under the same wave conditions. The wind only tests and wind only simulations are compared first to validate the simulation model with wind. The mean values of the results are shown in Table 8 for case B2 in the MWL. The simulation and test results for the time series under extreme wave and wind conditions are then compared. In the simulations, the measured wind time series were used as the input for the calculation of the drag on the tower. The force on the rotor was modelled as a constant thrust that was calculated from the mean wind velocity. This is because in extreme wind conditions, the wind drag on the tower is larger than that on the rotor. The mean drag on the rotor is around 73 kN under U=38 m/s, while the mean drag on the tower is 350 kN for the SUB mode, and 566 kN for the MWL mode. The wind time series can only be applied on the model one time in the simulation. It would be better to apply the wind time series on the tower. The simulation results and test results for sea state C3 in the MWL mode are plotted in Figure 19. The effect of wind on the motion in the time domain for case C3 in the SUB mode is shown in Figure 20. The simulation considered the $2^{nd}$ order wave effect. Since only constant and uniform wind conditions were considered, it is observed from the tests that only the mean values of the responses change due to the presence of wind. The numerical simulations give reasonable estimates of wind loads and induced motion responses. Further study is needed to investigate the behaviour of the STC in turbulent wind conditions.

## 6.7 Response statistics

The statistical values (mean, standard deviation, maximum and minimum) of the responses are important parameters that indicate the performance of the structure. In this section, the response statistics for different sea states are presented. The statistical values are the expected values of the statistics for all the realizations of the same sea state to reduce the statistical uncertainty. Each simulation corresponds to one hour in full scale. The statistical values from tests and simulation results of the MWL mode and the SUB mode in operational sea state (A1), extreme sea state I (A2) and II (A3) as well as the extreme sea state II + wind cases (C3) are presented in Figure 21-24 respectively. The simulation model considered the second order wave forces.

From Figure 21 to Figure 24, several conclusions can be made:

- In operational sea states, responses of motions and interface forces are significantly reduced in the SUB mode than those in the MWL mode. There are good comparisons between simulation and test results.
- In extreme sea states, there are large deviations between the simulation and test results for the MWL mode due to the strongly nonlinear phenomena, especially the motion and force peaks. The linear model over predicted the motion extremes while under predicted the forces extremes in the MWL mode. The responses of every channel are significantly greater than those under operational conditions.
- In extreme sea states with wind, the surge and pitch extremes in the wave propagation direction increase significantly in the presence of extreme wind. The surge and pitch responses caused by the wind in the SUB mode is smaller than that in the MWL mode. The effect of wind on the heave motion is negligible compared to that on the surge and pitch motions.

– The mean drift motion due to waves in the SUB mode is not significant, while the mean drift motion due to waves in the MWL mode much larger. However, the wind is the main source of the large mean drift motions in both modes in extreme conditions, especially for the SUB mode because there is insignificant mean wave drift.

The expected values of STDs for the realizations from tests and simulation results are compared and shown in Table 9. The values are calculated from (SIM.-TEST)/TEST. The differences are mostly under 10%, except for the wind case C3 for the SUB mode. This may be due to mean wind drag applied on the rotor, which should be dynamic wind drag calculated from wind time series. The STDs of the extreme cases for the MWL mode is not presented.

### 6.8 Extreme values estimation

The extreme values from tests and simulations for the MWL and SUB modes under sea states A3 and C3 are compared and shown in Table 10. The extreme values are the 1.3 times of the mean of the maxima of all the realizations for the extreme sea states II, i.e., A3 or C3, considering the sea states selection method. Such characteristic values can be considered as the long-term extreme values using the contour line method. The positive extremes (extreme +) and negative extremes (extreme -) in the cases with or without wind are all listed. The relative differences of the tests results between the MWL mode and SUB mode, which are calculated from (MWL-SUB)/SUB are presented. The differences between tests and simulation results under the SUB mode, which is calculated from (SIM.-TEST)/TEST are also shown.

All of the responses for the MWL mode are significantly greater than those for the SUB mode, and the relative differences for the forces are even greater (all are more than 350%) mainly due to the slamming impact forces. The test with wind shows a negative relative difference for pitch due to the wind-induced pitch that gives a positive extreme value in the MWL mode but a negative extreme value in the SUB mode. The comparison between simulation and tests results under the SUB mode shows the differences that are mostly under 20%, except cases that the test results are small.

Mooring tension extremes are critical values for the mooring system design. During the tests, there was dynamic effect for the mooring line 1. The mooring tension varied around the pretension applied, and the tension range of each realization for mooring line 2 and 3 under the extreme sea state A3 were estimated. The mean value and STD of these tension ranges are presented in Table 11, and the factor of 1.3 is applied. In the SUB mode, the mean value for the tension range is around 1/5 of that in the MWL mode. In this case, the fatigue damage for the mooring system will be significantly reduced in the SUB mode. But in the tests, all the mooring stiffness is assumed to be linear, i.e., the mooring line tension will be increased linearly with the horizontal displacement. In prototype catenary mooring system, the mooring stiffness is nonlinear.

## 7 Uncertainty analysis

All measurements include errors, and results are meaningless without knowledge of the level of errors. The total error of a measurement has two components: a fixed bias error and a random (precision) error. Bias errors are systematic errors, which are constant for the entire test. Bias errors are usually an accumulation of several individual bias errors, such as the incorrect calibration of the equipment, installation error of the testing model and improper use of the measurement device. Random errors are observed in repeated measurements that do not agree exactly and can be caused by several error sources, such as noise, external disturbances and other unknown sources. Random errors vary between different tests, and the error distribution can be measured by several precision indexes from repeated tests (ASME, 1985). As was suggested by the International Towing Tank Conference (ITTC) Quality Manual and Recommended Procedures (ITTC, 2008), a complete uncertainty analysis of test data should be performed, but due to the complexity of the model and tests as well as the time limitations and costs of the towing tank or ocean basin, it is difficult to quantify many error sources, such as the calibration error, installation error and model manufacturing error (Zhu et al., 2011). For offshore hydrodynamic tests, the Data Reduction Equation (DRE) is also difficult to establish. In this section, several important uncertainties factors in the numerical model and the testing model are identified and their effects on the interpretation of the test results are discussed.

Different model parameters will affect the numerical results. Significant influence is observed for the quadratic drag coefficients effects to the responses, but only in resonant region. The effect of the load cell existence on the responses is found to be insignificant. Also the effect of the 2nd order wave loads was found to have the marginal importance. These results are omitted in the paper. The mooring dynamic effects are analyzed and presented here.

There are also many factors that affect the accuracy of the model test results. The uncertainty in model fabrication and installation, as well as the uncertainty in the analysis of the regular and irregular wave test results are discussed in the following section.

### 7.1 Effect of mooring spring dynamics

Figure 7 and Figure 8 show that the mooring force is underestimated by the simulation model. This is due to the mooring dynamic effect, which was not accounted for in the numerical simulations. To estimate the dynamic effect of the mooring in the numerical simulations, a simple clump weight was added to mooring spring 1 to simulate the mass of the spring. The hydrodynamic excitations of the springs were not considered in the numerical model. In the model tests, the spring consisted of a distributed mass rather than a clumped mass, and the spring could experience transverse deformations that could not be simulated in the numerical model.

To consider the added mass, spring 1 was modelled as a 2 kg mass in model scale. Figure 25 shows the mooring force spectrum and compares the results between the tests and simulations with and without the mooring dynamic effect in the MWL mode for the operational sea state. The force spectrum for mooring line 1 shows that resonance of the clumped mass was excited with the 2 kg mass, and the resonant frequency (0.75 rad/s) was close to the special frequency (0.52 rad/s) that was observed in the tests. With the clumped mass in the simulations, the mooring line 1 force spectrum was reduced, while the force spectra for mooring lines 2 and 3 increased in the low frequency region compared to the cases without the clumped mass. This indicates that in the low frequency region, mooring lines 2 and 3 carry more tension, and mooring 1 carries less tension due to the presence of the clumped mass, which transfers some of the potential energy into kinetic energy. Because mooring line 1 was slightly inclined, the measured tension should be greater than the real horizontal tension, which means that the measured mooring line 1 force spectrum should be greater than in the real cases.

A dynamic mooring cable solver should be used to fully estimate the influence of the mooring system. In the simulation model, the clear spectral peak that shows the resonance of the clumped mass demonstrates that the special spectral peak observed in the test is mainly due to the dynamic effect of the spring. The underestimation of the mooring forces by the simulations might also be caused by neglecting the hydrodynamic excitations and the incline of the mooring springs caused by the large weight and long rope.

### 7.2 Uncertainty in model fabrication and installation

Careful checks and measurements were performed on the model fabrication and geometry. The random geometric error was approximately 1%, which is equivalent to an error of less than 1 cm for every 1 m. The weight precision was calculated from the static trim test as approximately 0.5%, which indicates that there is less than a 0.5 kg deviation from the required weight and draft.

The most critical parts of the installation and calibration of the test were the load cells. The total forces between two bodies were calculated based on all of the load cells assuming that every load cell measured the local force components (x, y and z) in the corresponding locations and directions (0º, 120º and 240º). Due to the relatively large size of the load cells, the real measurements were not exactly in the 0º, 120º and 240º directions. This did not affect the vertical force but caused bias errors in the horizontal forces. In addition, the installations of the load cells at the top of the torus were not exactly symmetric with those at the bottom of the torus.

As discussed previously, the mooring spring used in the test was also a source of bias error due to the large weight and the static deformation angle.

### 7.3 Uncertainty in regular and irregular wave test results

The regular wave recordings in the tests showed that the wave height was not completely stationary even under steady state conditions but included small fluctuations during the different cycles. The frequency was stable, but some cases contained higher order frequencies in the wave spectra. The responses had the same properties. To reveal the inherent variation in the regular wave tests, 20 cycles of responses were analyzed based on the test results. The scatters of the RAOs were evaluated with error bars to represent the STD values shown in Figure 7 and Figure 8. The coefficient of variation (CV) of the motion and force responses can be expressed as:

$$c_v = \sigma/\mu, \tag{5}$$

where $\sigma$ and $\mu$ are the standard deviation and mean value of the RAO, respectively, for all 20 cycles and can be expressed as:

$$\sigma = \sqrt{[\sum_1^N (x_i - \mu)^2]/(N-1)},\ \mu = \sum_1^N x_i /N \tag{6}$$

where $x_i$ is the RAO value for the i-th cycle; and N is the number of cycles, which is 20 in this case. The CVs of every channel for the regular wave periods (13 s and 21 s) for wave heights of 2 m and 9 m are shown in Table 12. For both periods, the CVs for the 9 m wave are smaller than those for the 2 m wave. One reason is the small relative random errors for the large wave. The relative random error can be expressed as $\varepsilon/\zeta$, where $\varepsilon$ is the random error, and $\zeta$ is the wave height. For a large wave with the same random error, the relative random error is small. The relative random error is larger for a small wave. The CVs for the RAOs of the mooring lines are quite large for small waves. In general, the mooring forces give higher errors than the other channels, which signify that the level of precision for the mooring forces is lower.

In the irregular wave tests, time series of approximately 100 min were recorded, and the last hour of data was analyzed to reduce the transient of the response at the beginning, so the random error due to the transient effect should be limited.

## 8 Concluding remarks and future work

This paper describes the model tests and the numerical simulations of the STC concept in two survival modes. The simulation and test results are compared, and the results for the SUB mode and MWL mode are also compared. The conclusions can be summarized as follows:

The test results show that strong nonlinear phenomena, such as slamming, green water and Mathieu instability, occur for the MWL mode, which are quite challenging for the structural integrity of the connection part of the spar and the torus due to the large impact forces. In addition, there are large pitch motions for the MWL mode, which induces large inertial loads in the system. In the SUB mode, the WEC is submerged in the water, which significantly reduces the extreme loads on the WEC, and the natural period of the heave motion is shifted outside of the range of frequent wave periods. Thus, the motions and forces between the bodies are significantly reduced. The SUB survival mode can be assumed to be a potential solution for ensuring survivability of the STC.

The numerical model agrees well with the model tests for the SUB mode. In the MWL mode, the simulation model can predict the response well if there are no strongly nonlinear phenomena, such as slamming and green water. Under extreme conditions, the simulation over-predicts the motions but under-predicts the forces. A nonlinear slamming model is needed to predict the slamming force and the effect on the motion responses.

The $2^{nd}$ order effect on the motions is not significant in the SUB survival mode of the STC concept, but is dominant for the MWL mode. The simulation model that considers only the $1^{st}$ order wave can predict the responses in the SUB mode. For the MWL mode, the simulation model that considers the $2^{nd}$ order wave should be used to predict the motions.

In the cases with wind, the wind-induced mean drift motion is much more significant than the $2^{nd}$ order mean drift motion in the SUB mode, while the wind-induced mean drift motion and wave-induced mean drift motion are both important in the MWL mode. The wind drag on the tower in extreme wind cases is larger than the wind drag on the disc. By using the drag disc in the tests, the rotational moment, gyroscopic effect and aerodynamic damping are not considered.

The interface forces between the spar and torus are not as sensitive as the motions to the $2^{nd}$ order slow drift effect. In the MWL mode, the forces are dominated by the first order wave force, and the $2^{nd}$ order wave force has an insignificant contribution to the interface forces under operational sea states, while in the extreme sea states, the slamming force excites the structural frequency responses. In the SUB mode, the interface forces are located in the wave frequency region, and the forces are significantly reduced by avoiding slamming impacts and reducing the wave excitation by completely submerging the torus.

The discrepancy in the mooring line forces between the simulations and tests suggests that if elastic springs are used to model the mooring system in future tests, the springs should be made as light as possible to reduce the inertia effects.

Several sources of uncertainty in the tests and numerical modeling are analyzed. Some sources of uncertainties are not presented due to the marginal importance. The existence of load cells in the numerical model does not have a significant effect on the responses, and the viscous drags only become significant when there is resonance.

Future work is needed in the study of survival modes: Which sea state should be defined as the survival mode, because it will affect how frequent will the survival mode be activated; Remote control is needed to activate the survival mode and if the survival mode is activated, how much time will it take to finish the transition phase between operational mode and survival mode;. It might also be possible to consider other alternative survival modes, e.g., in the survival sea states, a small PTO damping is applied; or the torus is not locked to the spar, but is submerged alone to change the excitation forces on the torus and its resonance period.

## 9 Acknowledgements

The authors gratefully acknowledge financial support from the European Commission through the 7th Framework Program (MARINA Platform –Marine Renewable Integrated Application Platform, Grant Agreement 241402), the Research Council of Norway through the Center for Ships and Ocean Structures (CeSOS), NTNU and the China Scholarship Council (CSC).

## 10 References

ASME, 1985. American National Standard. Part I: Measurement Uncertainty, Instruments and Apparatus. The Americal Society of Mechanical Engineering, New York.

Bak, C., Zahle, F., Bitsche, R., Kim, T., Yde, A., Henriksen, L.C., 2013. Description of the DTU 10 MW reference wind turbine, DTU Wind Energy Report-I-0092.
Cruz, J., 2008. Ocean wave energy. UK: Springer Series in Green Energy and Technology.
DNV, 2010. Recommended practice dnv-rp-c205, environmental conditions and environmental loads.
DNV, 2011. Wave Analysis by Diffraction and Morison Theory (WADAM), Sesam User Manual. V8.3.
Falcão, A.F.d.O., 2010. Wave energy utilization: A review of the technologies. Renewable and sustainable energy reviews 14 (3), 899-918.
Faltinsen, O., 1993. Sea loads on ships and offshore structures. Cambridge university press.
Fukushima Offshore Wind Consortium, 2013. Fukushima Floating Offshore Wind Farm Demonstration Project (Fukushima FORWARD), Construction of Phase I.
GOTO FOWT Website, 2015. http://goto-fowt.go.jp/english/home/spec/.
Goupee, A.J., Koo, B.J., Lambrakos, K.F., Kimball, R.W., 2012. Model tests for three floating wind turbine concepts, Offshore Technology Conference, OTC 23470, Texas, USA.
Haslum, H., Faltinsen, O., 1999. Alternative shape of spar platforms for use in hostile areas, Offshore technology conference. Offshore Technology Conference.
ITTC, 2008. Recommended Procedures and Guidelines-Testing and Extrapolation Methods, General Guidelines for Uncertainty Analysis in Resistance Towing Tank Tests.
Jonkman, J., 2010. Definition of the Floating System for Phase IV of OC3. Technical Report NREL/TP-500-47535.
Jonkman, J., Butterfield, S., Musial, W., Scott, G., 2009. Definition of a 5-MW Reference Wind Turbine for Offshore System Development, Technical Report/TP-500-38060. National Renewable Energy Laboratory.
Koo, B., Kim, M., Randall, R., 2004. Mathieu instability of a spar platform with mooring and risers. Ocean Engineering 31 (17), 2175-2208.
Li, L., Gao, Z., Moan, T., 2013. Joint environmental data at five european offshore sites for design of combined wind and wave energy devices, 32nd International Conference on Ocean, Offshore and Arctic Engineering, Nantes, France.
Luan, C., Michailides, C., Gao, Z., Moan, T., 2014. Modeling and analysis of a 5 MW semi-submersible wind turbine combined with three flap-type wave energy converters, 33rd International Conference on Ocean, Offshore and Arctic Engineering, San Francisco, USA.
MARINA Website, 2015. http://www.marina-platform.info/.
MARINTEK, 2007. SIMO User's Mannual Version 3.6.
MARINTEK, 2014. http://www.sintef.no/home/MARINTEK/Laboratories/The-Ship-Model-Tank/, be accessed on 13rd, February, 2014.
MAURO, H., 1960. The drift of a body floating on waves. Journal of ship research 4, 1-5.
Michailides, C., Luan, C., Gao, Z., Moan, T., 2014. Effect of Flap Type Wave Energy Converters on the Response of a Semi-Submersible Wind Turbine in Operational Conditions, 33rd International Conference on Ocean, Offshore and Arctic Engineering, San Francisco, USA.
Muliawan, M.J., Karimirad, M., Gao, Z., Moan, T., 2013a. Extreme responses of a combined spar-type floating wind turbine and floating wave energy converter (STC) system with survival modes. Ocean Engineering 65, 71-82.
Muliawan, M.J., Karimirad, M., Moan, T., 2013b. Dynamic response and power performance of a combined spar-type floating wind turbine and coaxial floating wave energy converter. Renewable energy 50, 47-57.
Muliawan, M.J., Karimirad, M., Moan, T., Gao, Z., 2012. STC (Spar-Torus Combination): A combined spar-type floating wind turbine and large point absorber floating wave energy converter—promising and challenging, 31st International Conference on Ocean, Offshore and Arctic Engineering. American Society of Mechanical Engineers, pp. 667-676.
Naess, A., Moan, T., 2013. Stochastic dynamics of marine structures. Cambridge University Press.
Pinkster, J.A., 1975. Low-frequency phenomena associated with vessels moored at sea. Society of Petroleum Engineers Journal 15 (06), 487-494.
Principle Power Website, 2015. http://www.principlepowerinc.com/products/windfloat.html.
Salter, S.H., Taylor, J., Caldwell, N., 2002. Power conversion mechanisms for wave energy. Proceedings of the Institution of Mechanical Engineers, Part M: Journal of Engineering for the Maritime Environment 216 (1), 1-27.
Stiesdal, H., 2009. Hywind: The world’s first floating MW-scale wind turbine. Wind directions, Dec.
The European Wind Energy Association, 2015. The European offshore wind industry - key trends and statistics 2014. A report by the European Wind Energy Association.
The World Wind Energy Association, 2014. World Wind Resource Assessment Report WWEA Technical Paper Series (TP-01-14).
Wan, L., Gao, Z., Moan, T., 2014. Model test of the STC concept in survival modes, 33rd International Conference on Ocean, Offshore and Arctic Engineering. American Society of Mechanical Engineers.

WaveBob, 2014. http://en.wikipedia.org/wiki/Wavebob, be accessed in 2nd, January, 2014.

Winterstein, S., Ude, T., Cornell, C., Bjerager, P., Haver, S., 1993. Environmental parameters for extreme response: Inverse FORM with omission factors, Proceedings ICOSSAR.

Zhu, S., Wu, M., Moan, T., 2011. Experimental and numerical study of wave-induced load effects of open ships in oblique seas. Journal of ship research 55 (2), 100-123.

# Table

Table 1. Froude scaling of the variables.

| Variables | Symbol | Scale factor | Value |
|---|---|---|---|
| Linear Dimensions | D | $\lambda$ | 1:50 |
| Fluid or structure velocity | u | $\lambda^{1/2}$ | 1:7.07 |
| Fluid or structure acceleration | a | 1 | 1:1 |
| Time or period | t | $\lambda^{1/2}$ | 1:7.07 |
| Structure mass | m | $\lambda^{3}$ | $1:1.25\times10^{5}$ |
| Structure displacement volume | V | $\lambda^{3}$ | $1:1.25\times10^{5}$ |
| Force | F | $\lambda^{3}$ | $1:1.25\times10^{5}$ |
| Moment | M | $\lambda^{4}$ | $1:6.25\times10^{6}$ |

Table 2. STC dimensions.

| Spar and Tower | | [m] |
|---|---|---|
| Lower part of spar | Diameter | 10 |
| | Length | 108 |
| Upper part of spar | Diameter | 6.45 |
| | Length | 24 |
| Tower | Diameter | 5.5 |
| | Length | 77 |
| Torus | | |
| | Height | 8 |
| | Outer diameter | 20 |
| | Inner diameter | 8 |

Table 3. Drafts of the model for the different survival modes.

| | MWL mode [m] | SUB mode [m] |
|---|---|---|
| Spar and Tower | 122 | 148 |
| Torus | 4 | 30 (From Torus bottom to the MWL) |

Table 4. Weight data for the single-body model and the two-body model.

| STC | | MWL mode | SUB mode |
|---|---|---|---|
| Total weight (including ballast) [ton] | | 10,036.25 | 11,840.00 |
| Ballast [ton] | | 4276.25 | 6080.00 |
| C.O.G. from WL [m] | | 67.50 | 100.00 |
| C.O.G. from geometric center of torus [m] | | 67.50 | 74.00 |
| Radius of gyration w.r.t. WL [m] | Rxx | 88.50 | 114.00 |
| | Ryy | 88.50 | 114.00 |
| | Rzz | 4.50 | 4.50 |
| Spar and Tower | | | |
| Total weight (including ballast) [ton] | | 8891.25 | 10,695.00 |
| Ballast [ton] | | 4276.25 | 6080.00 |
| C.O.G. from WL [m] | | 76.50 | 108.00 |
| Radius of gyration w.r.t. WL [m] | Rxx | 94.50 | 120.00 |
| | Ryy | 94.50 | 120.00 |
| | Rzz | 4.00 | 4.00 |
| Torus | | | |
| Total weight [ton] | | 1145.00 | 1145.00 |
| Ballast [kg] | | - | - |
| C.O.G. from WL [m] | | 0.00 | 0.00 |
| Radius of gyration w.r.t. WL [m] | Rxx | 7.00 | 26.50 |
| | Ryy | 7.00 | 26.50 |
| | Rzz | 7.00 | 7.00 |

Table 5. Decay test results.

| | SUB | | | | MWL | | | |
|---|---|---|---|---|---|---|---|---|
| D.O.F. | $T_m$ [s] | $T_f$ [s] | $\xi$ | $T_{fs}$ | $T_m$ [s] | $T_f$ [s] | $\xi$ | $T_{fs}$ |
| SURGE | 14.42 | 102 | 0.034 | 106 | 13.86 | 98 | 0.04 | 104 |
| SWAY | 13.09 | 93 | 0.046 | - | 13.17 | 93 | 0.04 | - |

| | | | | | | | | |
|---|---|---|---|---|---|---|---|---|
| HEAVE | 6.67 | 47 | 0.024 | 47 | 1.81 | 13 | 0.07 | 12 |
| ROLL | 3.62 | 26 | 0.027 | - | 5.09 | 36 | - | - |
| PITCH | 3.63 | 26 | 0.023 | 26 | 5.18 | 37 | - | 39 |
| Comments: $T_m$ are the identified natural periods from tests in model scale; $\xi$ are the damping ratios obtained from the decay tests; $T_f$ are full scale values of $T_m$; $T_{fs}$ are the natural periods calculated by numerical model in full scale. | | | | | | | | |

Table 6. Regular wave test matrix and the occurrence of nonlinear phenomenon (Colored background).

| Test mode | MWL | | SUB | |
|---|---|---|---|---|
| H [m] / T [s] | 2 | 9 | 2 | 9 |
| 7 | | - | | - |
| 9 | | Slamming and green water | | |
| 11 | | | | |
| 12 | Slamming | | - | - |
| 13 | | | | |
| 14 | | | - | - |
| 15 | | | | |
| 17 | | Mathieu instability | | |
| 19 | | | | |
| 21 | | | | |
| 23 | | | | VIM |
| 25 | - | - | - | |
| Comment: '-' indicates no wave test for this period | | | | |

Table 7. Irregular wave and wind test matrix.

| | Sea States | Hs [m] | Tp [s] | Uw [m/s] | Realization | Case no. |
|---|---|---|---|---|---|---|
| Irregular wave only | Operational | 2.75 | 11.0 | - | 6 (SUB); 3 (MWL) | A1 |
| | Extreme 1 | 13.5 | 15.0 | - | 6 (SUB); 3 (MWL) | A2 |
| | Extreme 2 | 15.3 | 15.5 | - | 6 (SUB); 6 (MWL) | A3 |
| Wind only | Operational | - | - | 11.4 (large disc) | 1 (SUB); 1 (MWL) | B1 |
| | Extreme | - | - | 33.3 (small disc) | 1 (SUB); 1 (MWL) | B2 |
| Irregular wave only+wind | Operational | 2.75 | 11.0 | 11.4 (large disc) | 3 (SUB); 3 (MWL) | C1 |
| | Extreme 1 | 13.5 | 15.0 | 33.3 (small disc) | 3 (SUB); 0 (MWL) | C2 |
| | Extreme 2 | 15.3 | 15.5 | 33.3 (small disc) | 3 (SUB); 3 (MWL) | C3 |

Table 8. Comparison of mean values from the simulations and tests under extreme wind conditions B2 for wind only test for the MWL mode.

| MEAN VALUE | SURGE [m] | HEAVE [m] | PITCH [degree] |
|---|---|---|---|
| TEST | -17.94 | 0.01 | 6.0 |
| SIMULATION | -18.36 | -0.04 | 6.5 |

Table 9. Comparison of the mean values of STDs between tests and simulations in the MWL and SUB survival modes.

| | SURGE | HEAVE | PITCH | FX | FZ |
|---|---|---|---|---|---|
| OPERATIONAL SEA STATE (SUB, A1) | 8% | -3% | 3% | -5% | 7% |
| EXTREME SEA STATE I (SUB, A2) | 1% | -7% | -1% | -8% | 1% |
| EXTREME SEA STATE II (SUB, A3) | 0% | -6% | -1% | -7% | 1% |
| EXTREME SEA STATE II + WIND (SUB, C3) | 27% | -2% | 9% | -4% | 3% |
| OPERATIONAL SEA STATE (MWL, A1) | -8% | -11% | 1% | 0% | -11% |

Table 10. Comparison of the extreme values from tests and simulations in the MWL and SUB survival modes.

| Survival mode | Channels | Extreme + (Maximum) | Extreme - (Minimum) |
|---|---|---|---|

| | | TEST (NO WIND) | SIM. (NO WIND) | TEST (WIND) | SIM. (WIND) | TEST (NO WIND) | SIM. (NO WIND) | TEST (WIND) | SIM. (WIND) |
|---|---|---|---|---|---|---|---|---|---|
| SUB | SURGE [m] | 12.92 | 14.81 | -1.24 | 4.44 | -18.87 | -17.20 | -26.35 | -28.85 |
| | HEAVE [m] | 5.25 | 4.58 | 4.55 | 4.57 | -6.48 | -5.75 | -6.38 | -5.70 |
| | PITCH [degree] | 7.89 | 7.54 | 9.26 | 9.69 | -6.08 | -6.43 | -3.71 | -4.90 |
| | FX [kN] | 2102.86 | 2096.20 | 2586.35 | 2650.81 | -2381.09 | -2141.33 | -2073.33 | -1843.52 |
| | FZ [kN] | 4912.78 | 5540.65 | 4654.81 | 5455.35 | -6676.89 | -5652.55 | -6564.01 | -5522.89 |
| MWL | SURGE [m] | 13.07 | 11.78 | -12.40 | -14.85 | -42.58 | -90.28 | -57.23 | -102.32 |
| | HEAVE [m] | 17.27 | 16.90 | 14.14 | 17.31 | -17.93 | -22.39 | -11.96 | -22.10 |
| | PITCH [degree] | 16.84 | 39.19 | 21.96 | 41.88 | -7.84 | -8.26 | 2.14 | 2.50 |
| | FX [kN] | 11949.77 | 2326.41 | 12317.27 | 2746.65 | -16610.39 | -10453.32 | -18933.67 | -10446.40 |
| | FZ [kN] | 31953.62 | 28001.43 | 30465.94 | 25611.77 | -77764.41 | -29151.31 | -86671.85 | -27495.25 |
| Relative Diff. (Test): (MWL-SUB)/SUB | SURGE | 1% | - | 901% | - | 126% | - | 117% | - |
| | HEAVE | 229% | - | 211% | - | 177% | - | 87% | - |
| | PITCH | 113% | - | 137% | - | 29% | - | -158% | - |
| | FX | 468% | - | 376% | - | 598% | - | 813% | - |
| | FZ | 550% | - | 555% | - | 1065% | - | 1220% | - |
| Relative Diff. (SUB) : (SIM.-TEST)/TEST | SURGE | | 15% | | -459% | | -9% | | 9% |
| | HEAVE | | -13% | | 1% | | -11% | | -11% |
| | PITCH | | -4% | | 5% | | 6% | | 32% |
| | FX | | 0% | | 2% | | -10% | | -11% |
| | FZ | | 13% | | 17% | | -15% | | -16% |

Table 11. The mean value and STD of tension ranges under extreme sea state A3

| Under extreme sea states (6 realizations) | MWL | | SUB | |
|---|---|---|---|---|
| | MEAN | STD | MEAN | STD |
| Mooring line 2, tension mean range (kN) | 1296 | 135 | 285 | 51 |
| Mooring line 3, tension mean range (kN) | 1203 | 126 | 287 | 45 |

Table 12. Coefficients of variation for the RAOs of motions and forces for two wave periods for wave heights of 2 m and 9 m.

| RAO of channels | | SURGE | HEAVE | PITCH | FX | FZ | M1 | M2 | M3 |
|---|---|---|---|---|---|---|---|---|---|
| H=2 m | T=13 s | 3.1% | 1.7% | 3.0% | 2.8% | 2.0% | 3.6% | 17.4% | 12.0% |
| | T=21 s | 3.4% | 1.7% | 4.1% | 2.5% | 2.2% | 7.4% | 10.9% | 12.0% |
| H=9 m | T=13 s | 0.8% | 1.0% | 0.8% | 0.9% | 1.0% | 1.2% | 3.7% | 3.5% |
| | T=21 s | 0.7% | 0.7% | 0.6% | 0.8% | 1.0% | 1.3% | 3.0% | 2.2% |

**Figure**

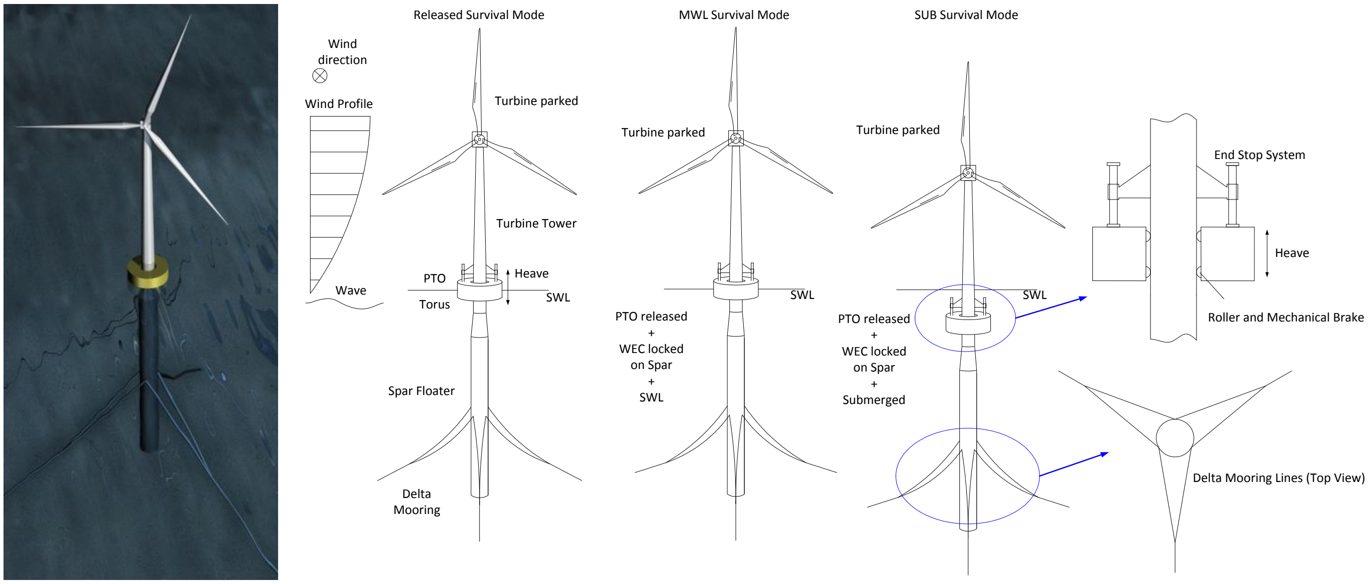


Figure 1. STC concept and proposed survival modes.

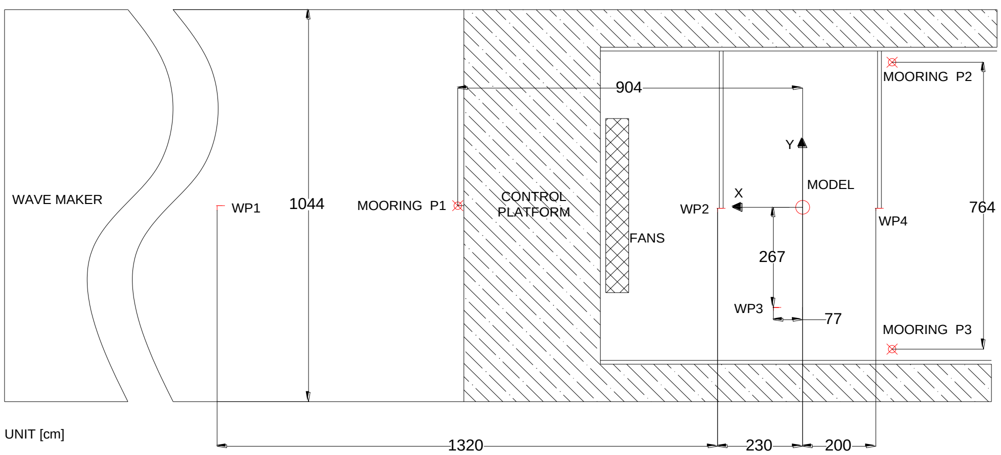


Figure 2. Top view of the layout for the test facility.

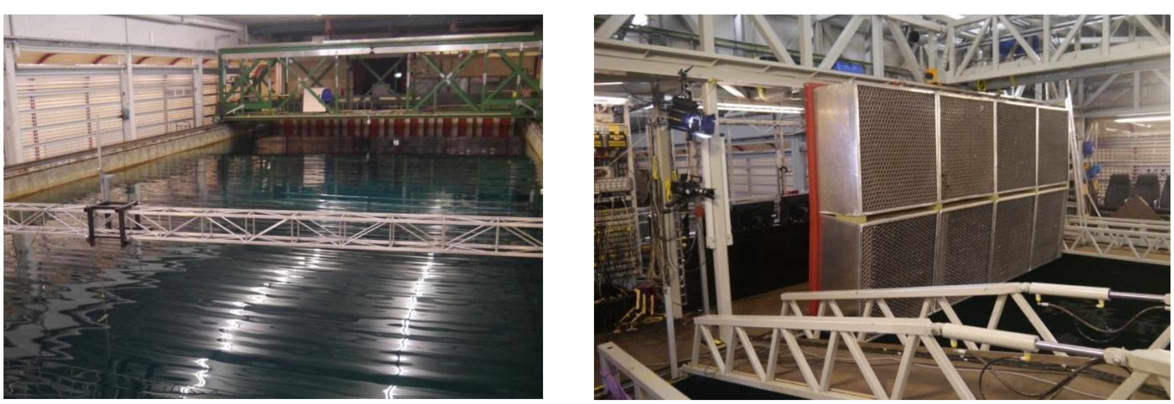

Figure 3. Test facilities. The left picture shows the wave maker, and the right picture shows the fans that generate the wind and the control platform.

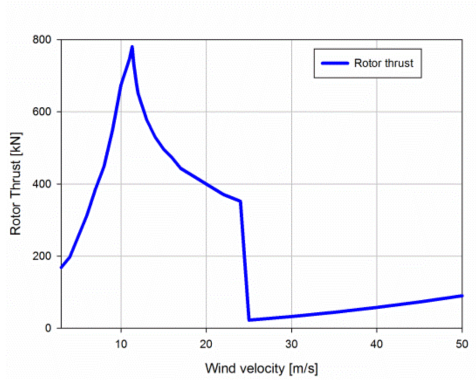

Figure 4. Wind turbine thrust curve with different wind velocity at the nacelle position in full scale

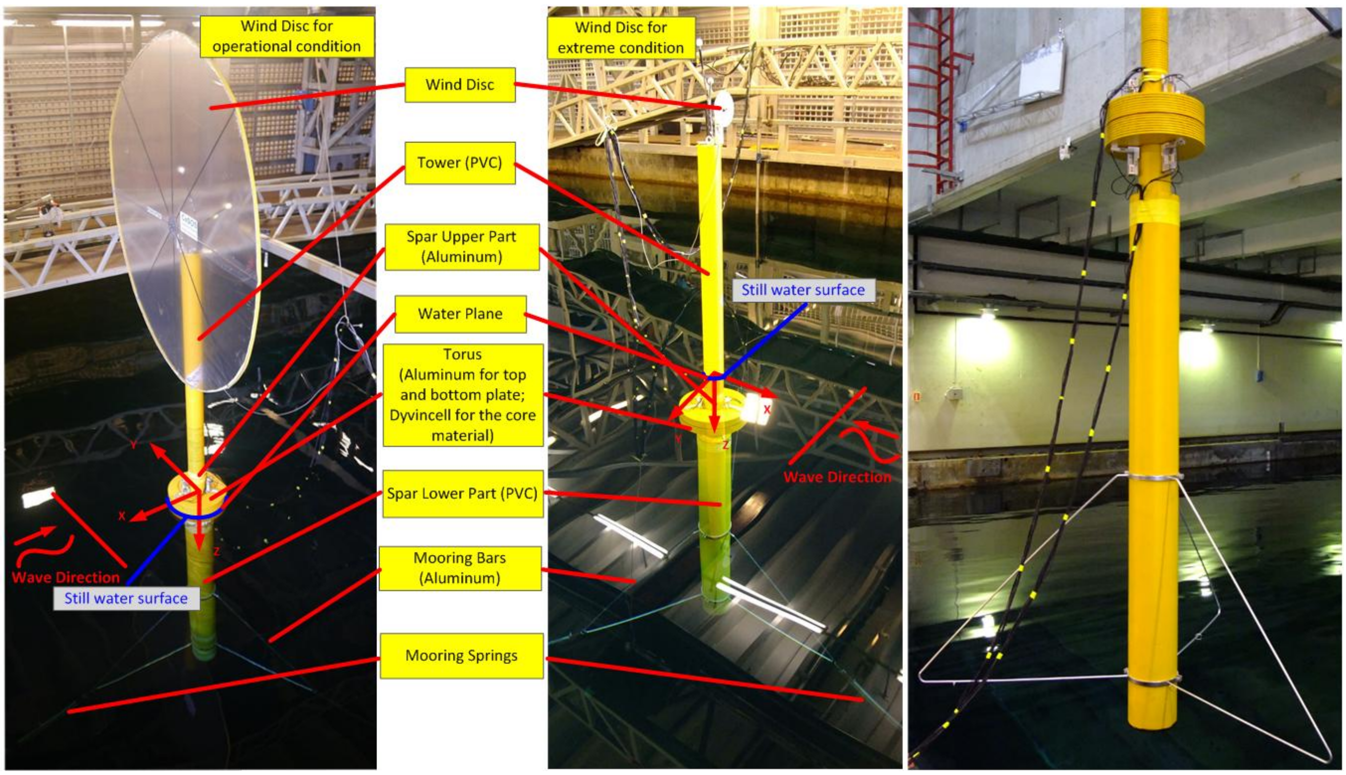

Figure 5. STC model, coordinate systems and different parts of the model in the two survival modes.

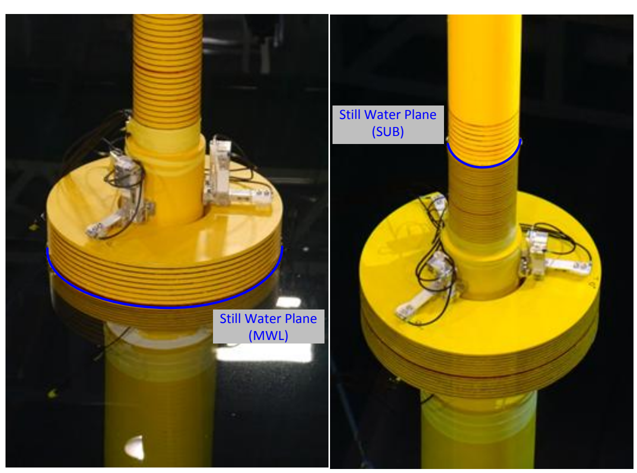

Figure 6. Load cell configurations for the two survival modes (a similar arrangement of load cells was present on the bottom of the torus).

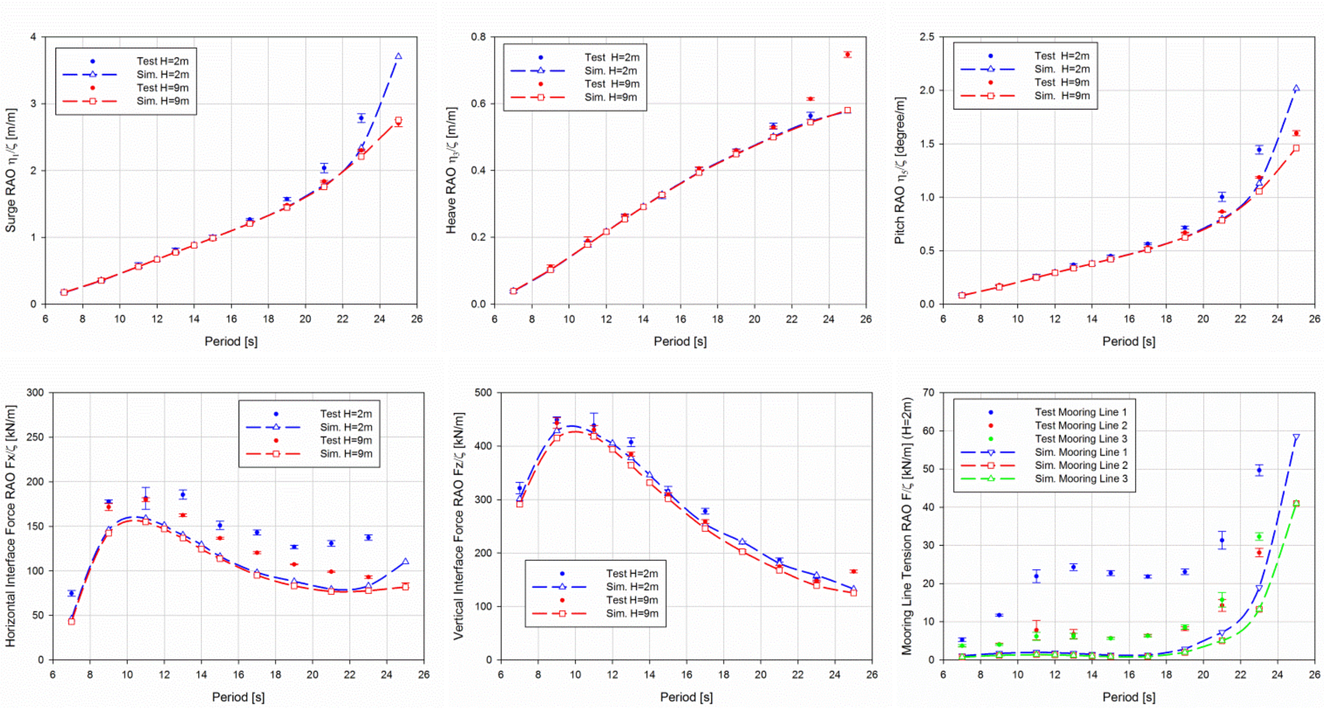


Figure 7. RAOs for motions and forces in the simulations and tests for the SUB mode.

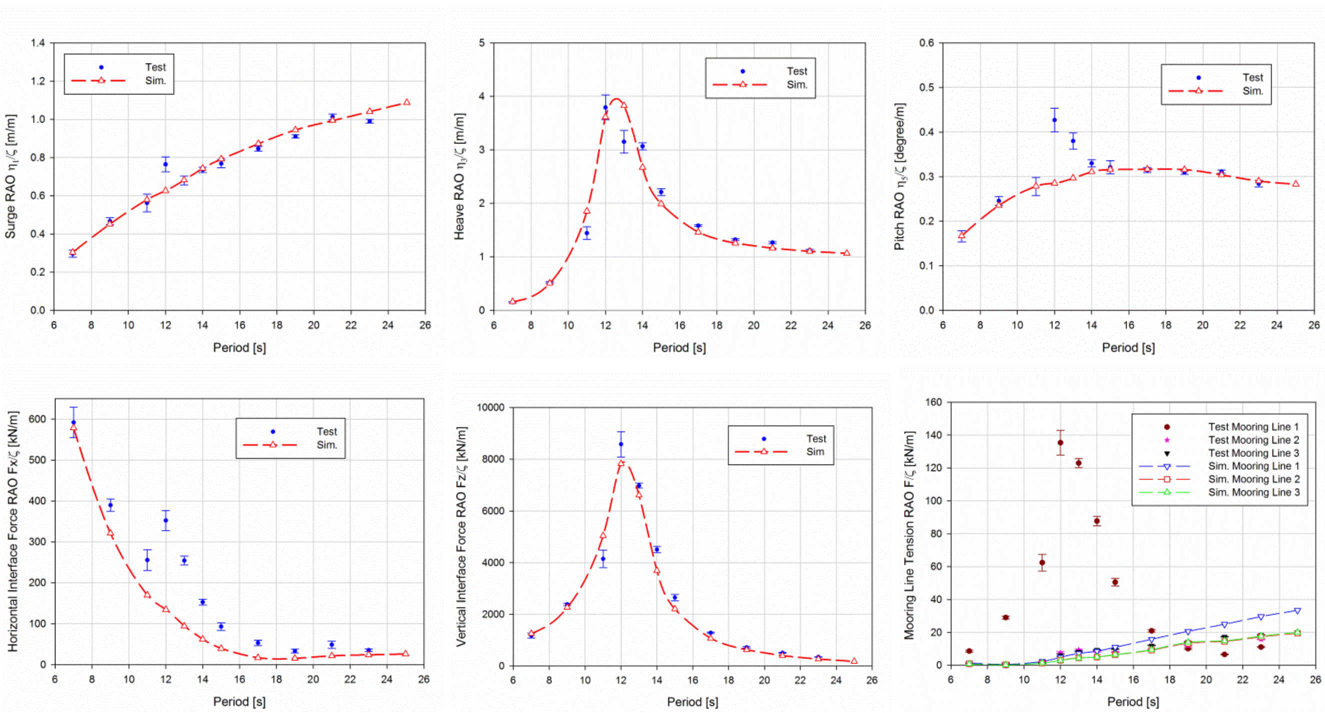


Figure 8. RAOs for motions and forces in the simulations and tests for the MWL mode.

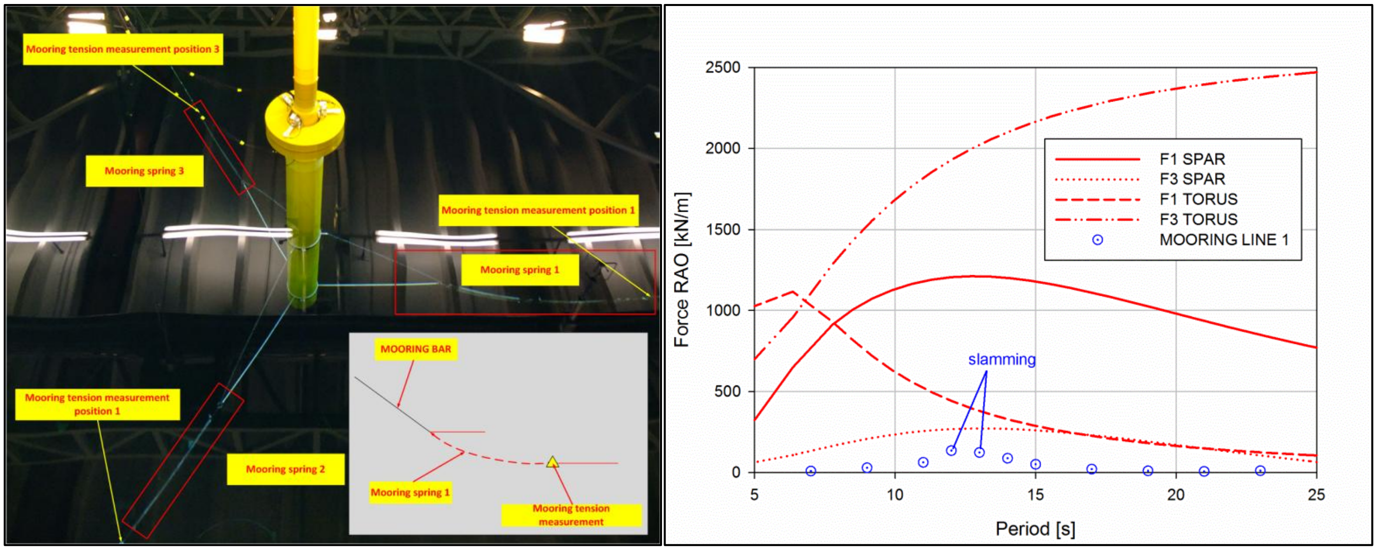


Figure 9. Mooring layout (left) and force RAO comparisons between the dynamic force of mooring line 1 and the excitation forces in surge and heave directions of the spar and the torus in MWL mode (right).

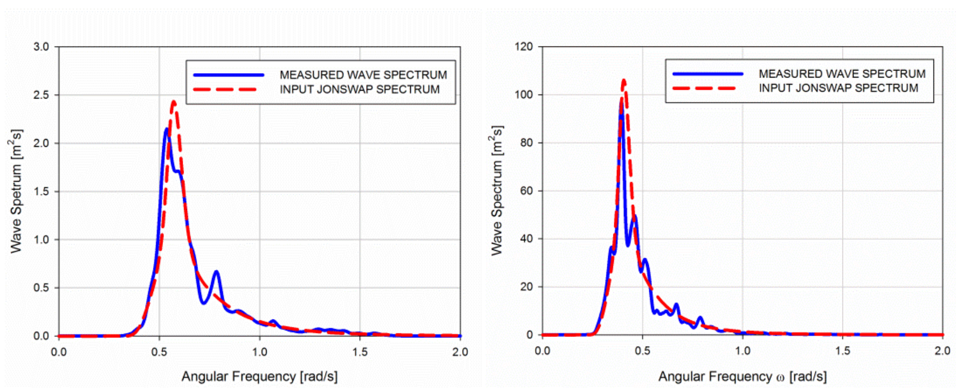


Figure 10. Comparison between the wave spectrum and target spectrum in operational sea states (left) and extreme sea states (right).

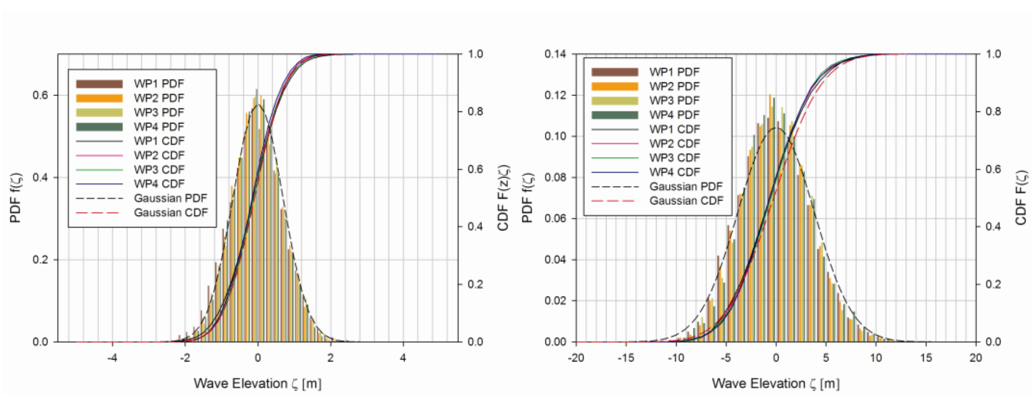


Figure 11. Probability distribution function and cumulative distribution function of the wave elevation in operational sea states (left) and extreme sea states (right).

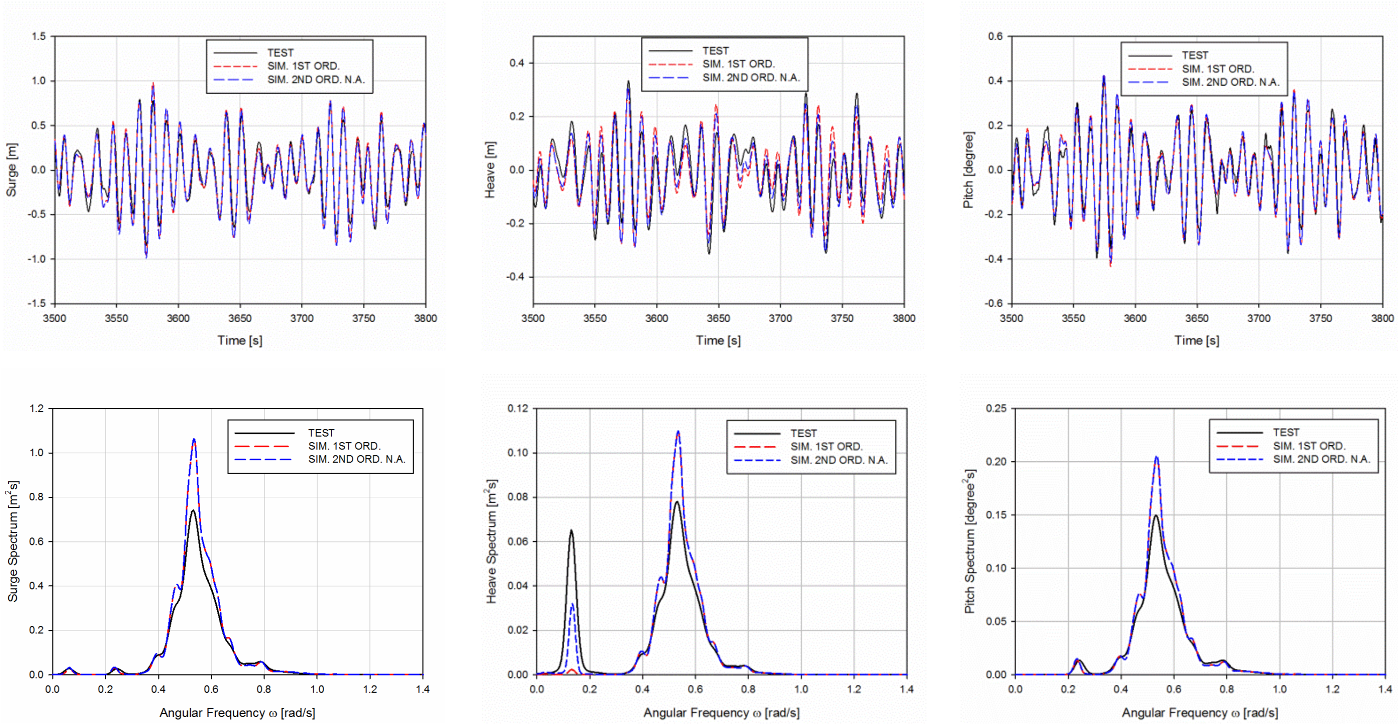


a) Surge time series and spectrum. b) Heave time series and spectrum. c) Pitch time series and spectrum.

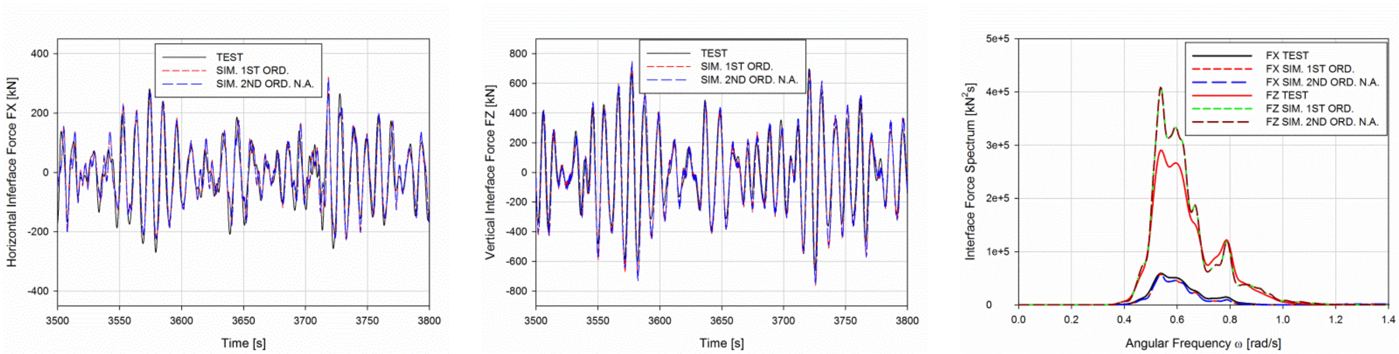


d) Fx time series. e) Fz time series. f) Fx and Fz spectra.

Figure 12. Comparisons of the motion and interface force responses in the time and frequency domains between the numerical simulations and model tests for operational condition A1 in the SUB mode.

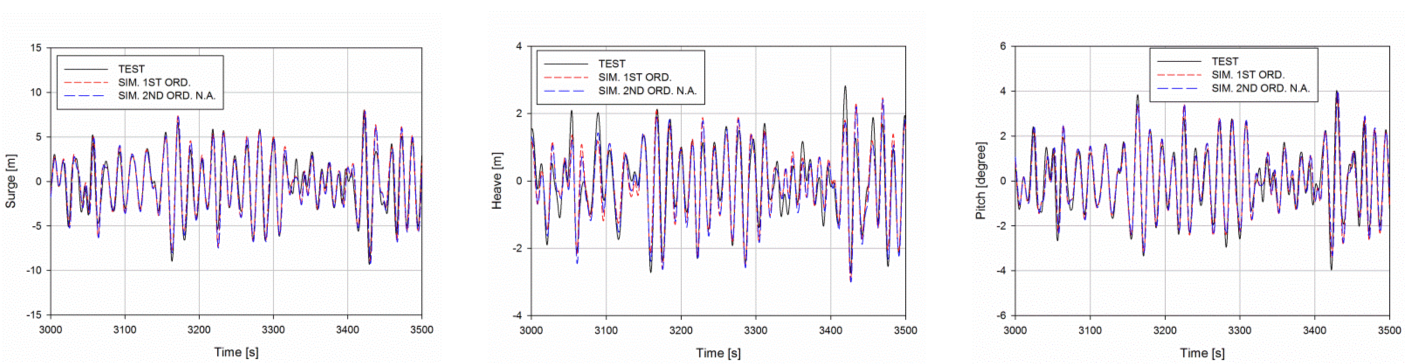

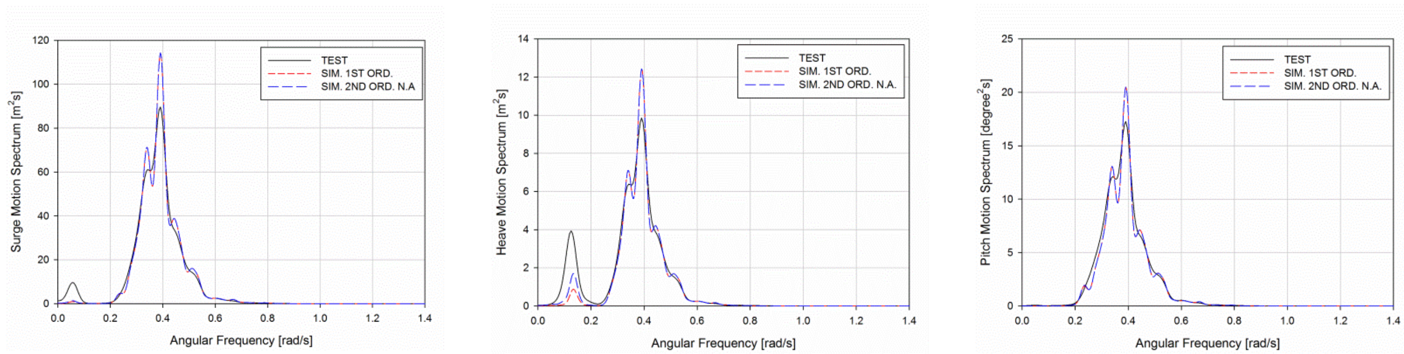


a) Surge time series and spectrum. b) Heave time series and spectrum. c) Pitch time series and spectrum.

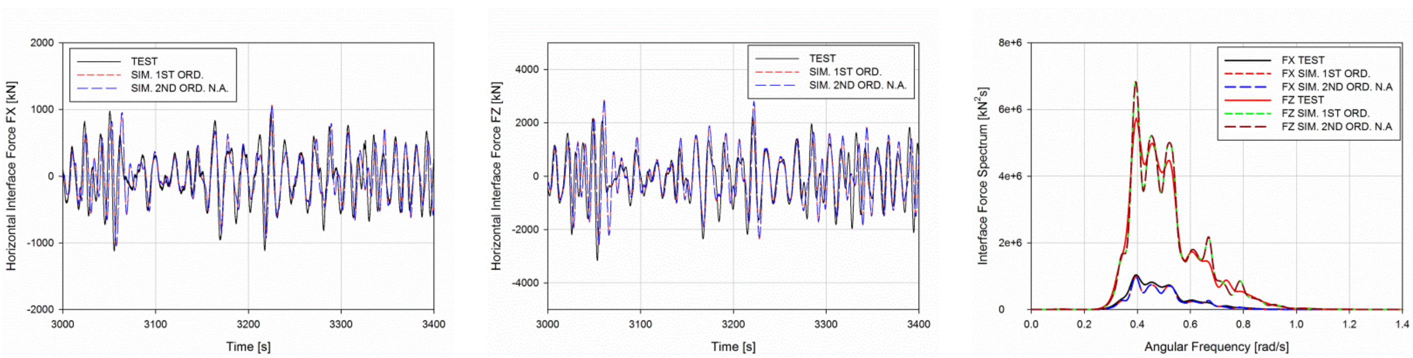


d) Fx time series. e) Fz time series. f) Fx and Fz spectra.

Figure 13. Comparisons of the motion and interface force responses in the time and frequency domains between the numerical simulations and model tests for extreme condition A3 in the SUB mode.

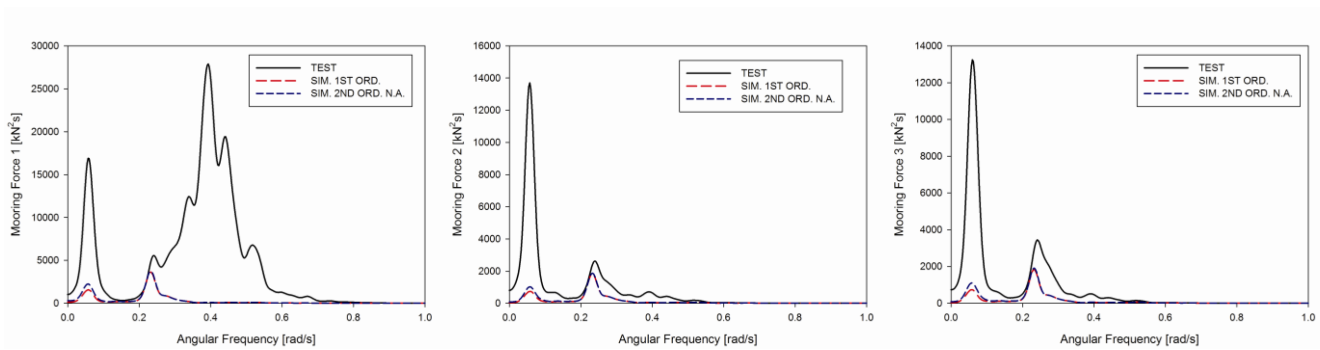


Figure 14. Mooring force spectra from tests and simulations based on the 1st order and 2nd order wave force in the SUB mode.

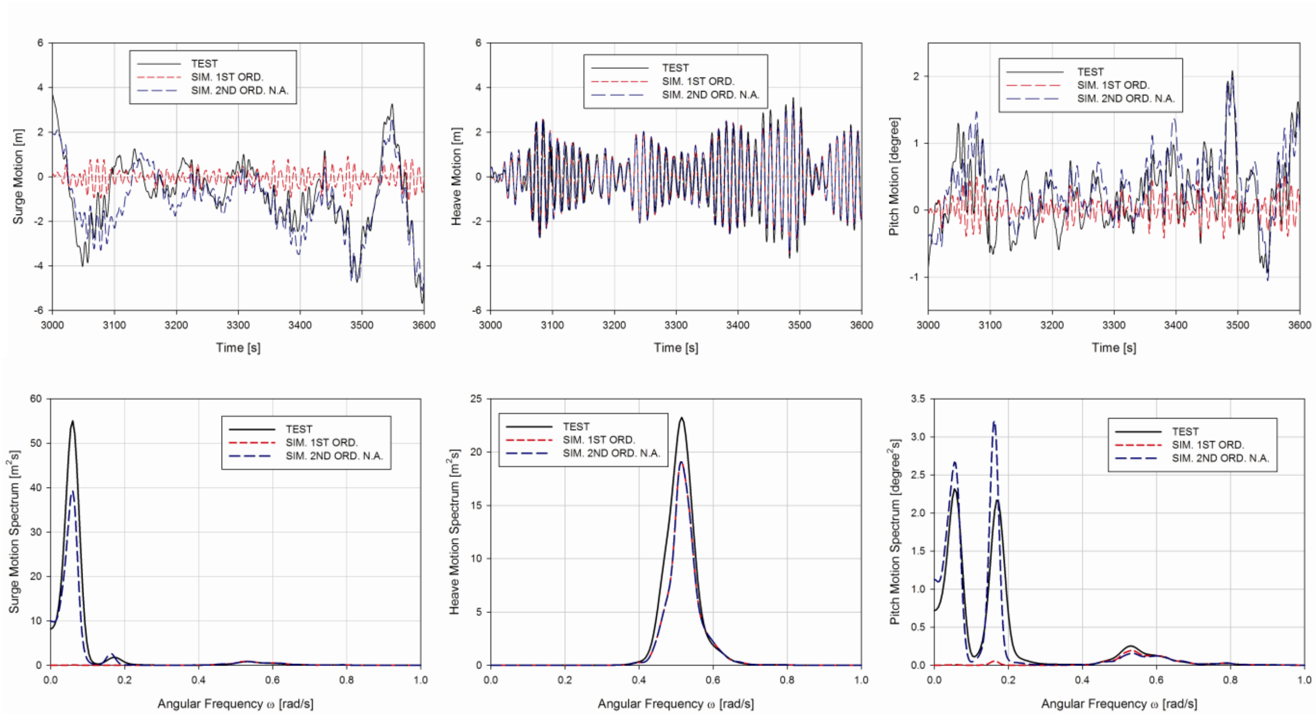


Figure 15. Comparisons of the motion responses in the time and frequency domains between the numerical simulations and model tests for extreme condition A1 in the MWL mode.

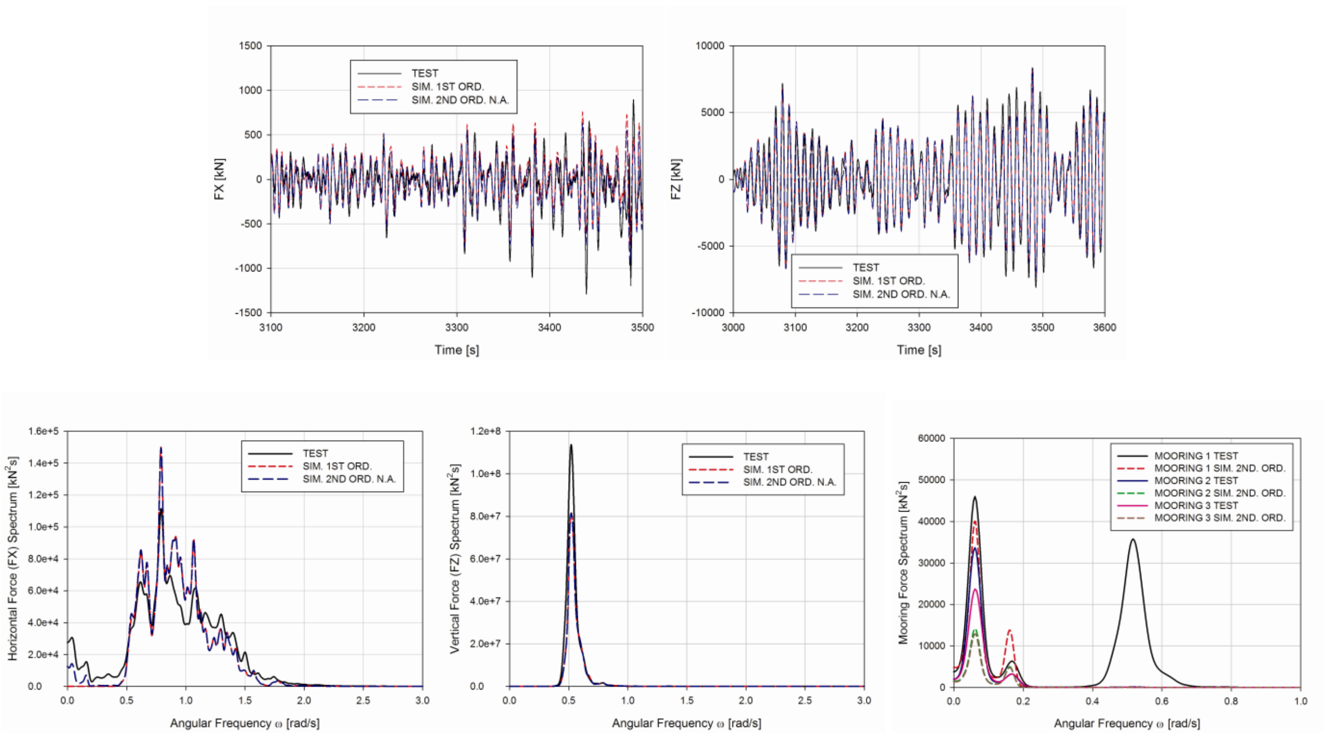


Figure 16. Comparisons of the interface force and mooring line tension responses in the time and frequency domains between the numerical simulations and model tests for extreme condition A1 in the MWL mode.

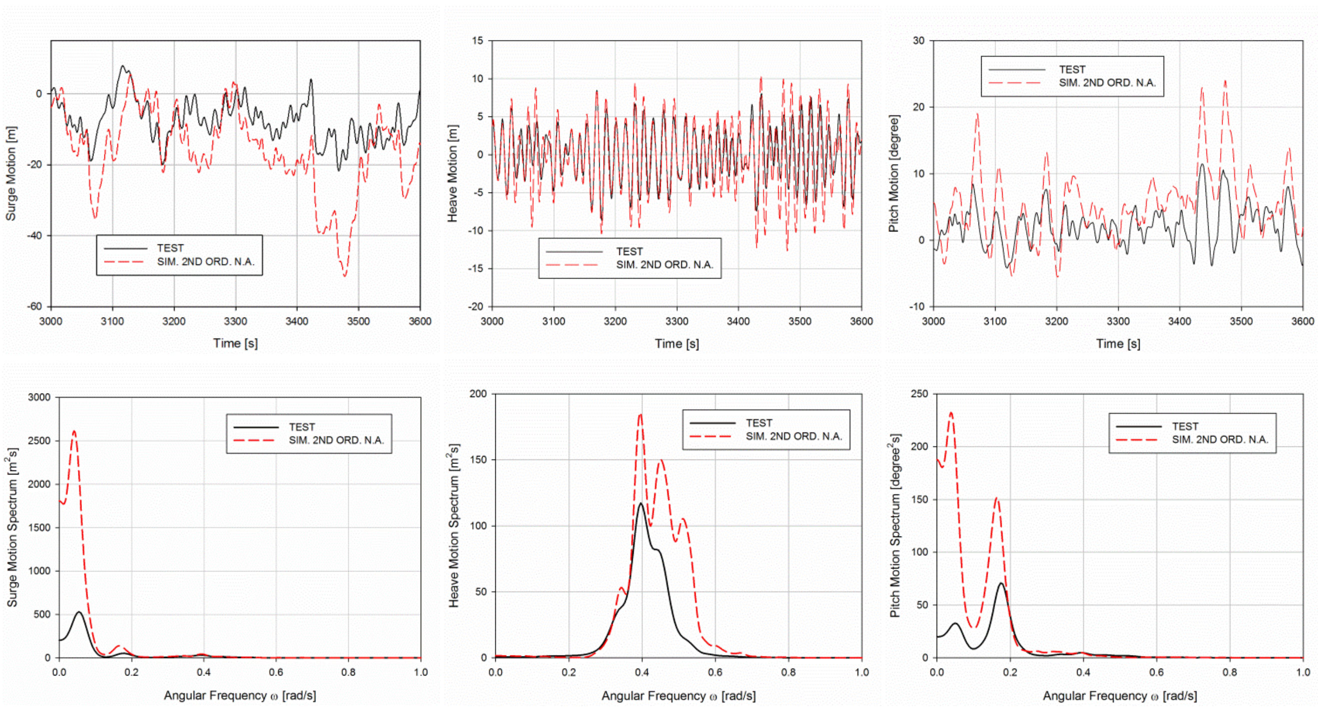


Figure 17. Comparisons of the motion responses of the tests and simulations in the time and frequency domains for extreme sea state A3 in the MWL mode.

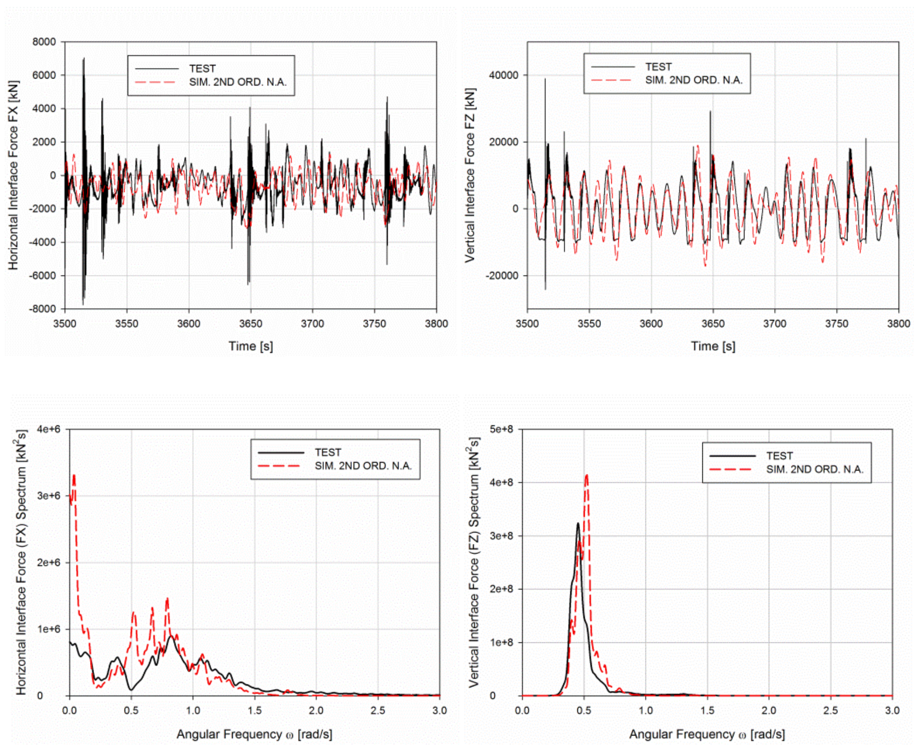


Figure 18. Comparisons of the force responses of the tests and simulations in the time and frequency domains for extreme sea state A3 in the MWL mode.

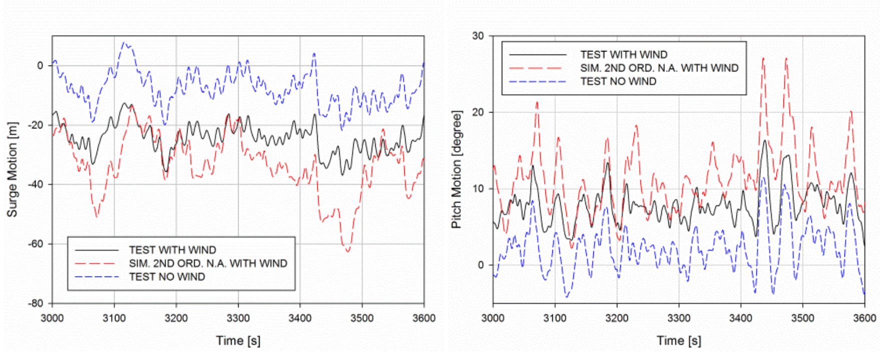


Figure 19. Wind effects on the surge and pitch motions for environmental conditions C3 (wave+wind) and A3 (wave only) in the MWL mode.

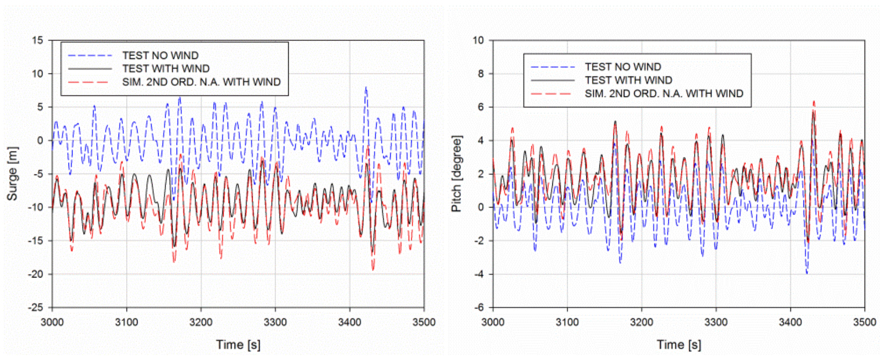


Figure 20. Wind effects on the surge and pitch motions for environmental conditions C3 (wave+wind) and A3 (wave only) in the SUB mode.

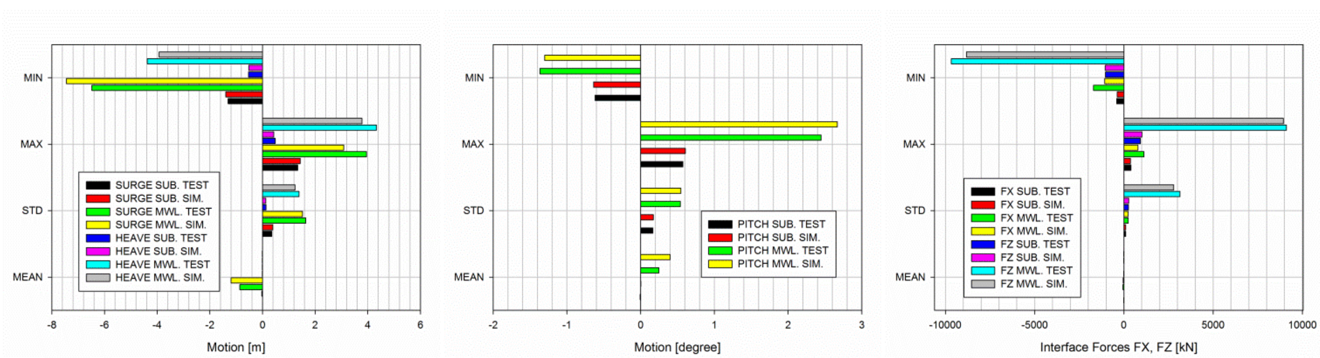


Figure 21. Response statistics (mean, STD, max. and min.) of test and simulation results in operational sea states (A1) under the MWL mode and SUB mode.

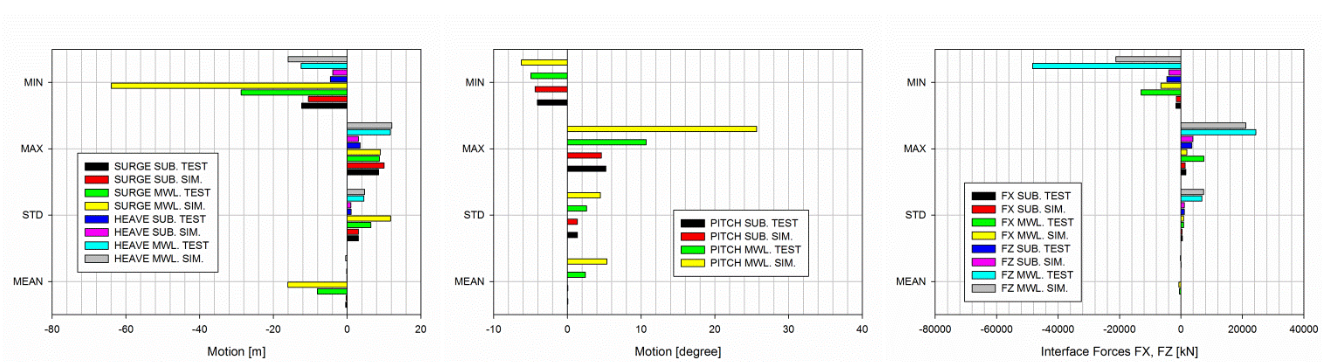


Figure 22. Response statistics (mean, STD, max. and min.) test and simulation results in extreme sea states I (A2) under the MWL mode and SUB mode.

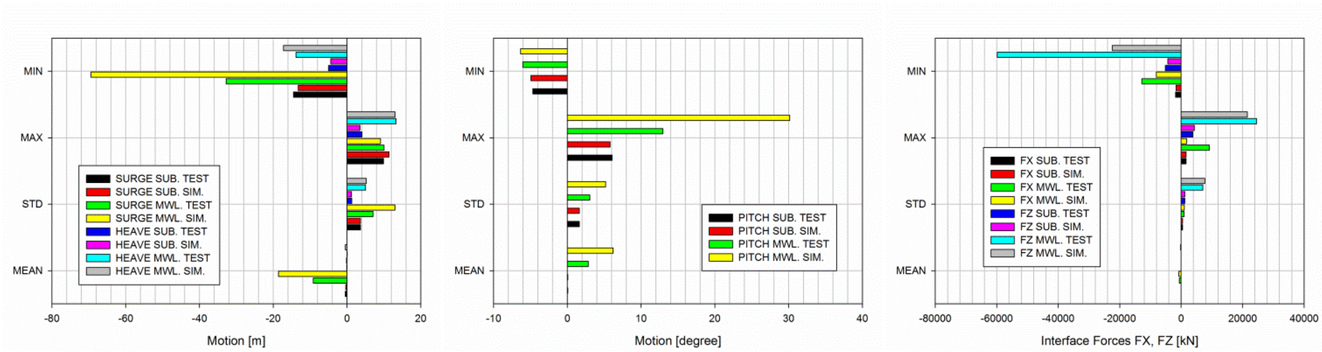


Figure 23. Response statistics (mean, STD, max. and min.) test and simulation results in extreme sea states II (A3) under the MWL mode and SUB mode.

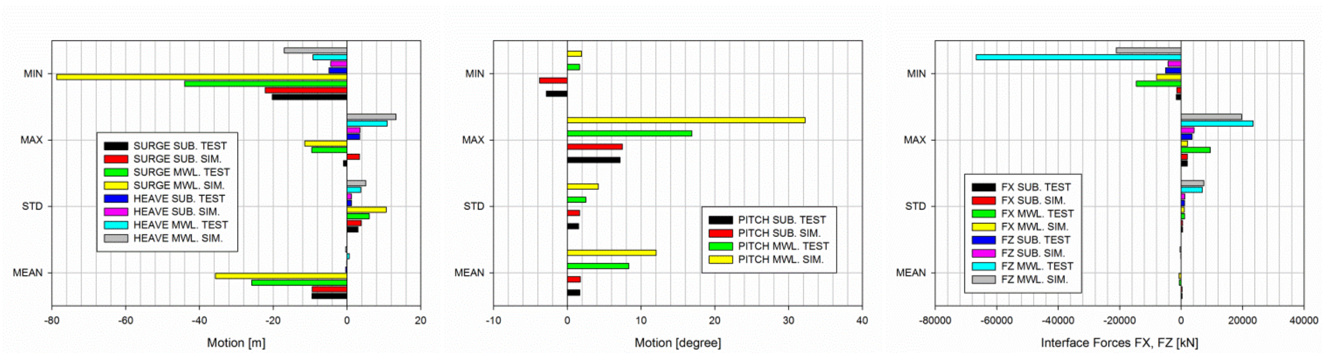


Figure 24. Response statistics (mean, STD, max. and min.)  test and simulation results in extreme sea states II +  wind case (C3) under the MWL mode and SUB mode.

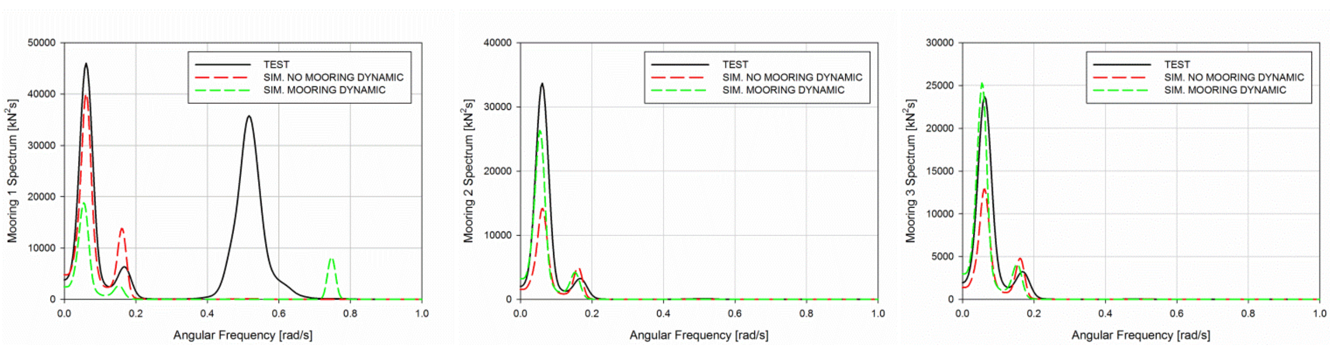


Figure 25. Spectra of mooring line forces in the tests and simulations with and without the mooring dynamic effect in the operational sea state in the MWL mode.